Title
PARTICLE CORRELATIONS IN PROTON-NUCLEUS AND NUCLEUS-NUCLEUS COLLISIONS

Author
Nagamiya, S.

Publication Date
1982-02-01

LBL-14034
Preprint

Lawrence Berkeley Laboratory
UNIVERSITY OF CALIFORNIA

Submitted to the Soviet Journal of Particles and Nuclei

PARTICLE CORRELATIONS IN PROTON-NUCLEUS AND NUCLEUS-NUCLEUS COLLISIONS

Shoji Nagamiya

February 1982

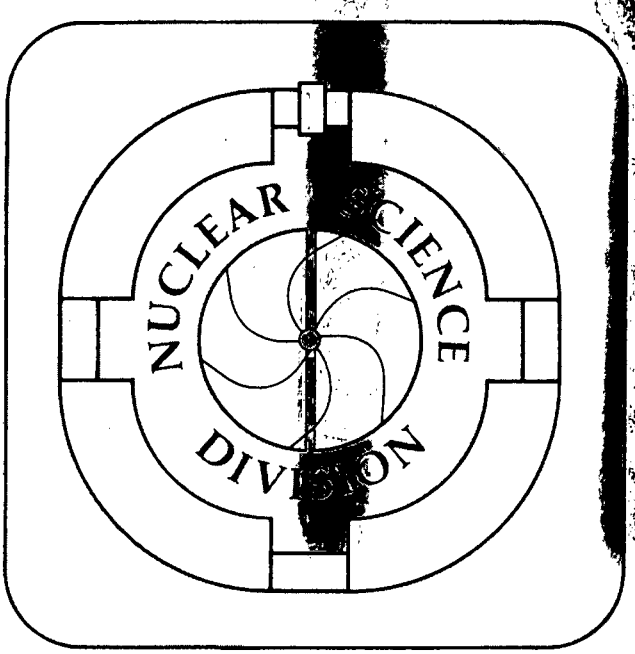

Prepared for the U.S. Department of Energy under Contract W-7405-ENG-48

DISCLAIMER

Particle Correlations in Proton–Nucleus and Nucleus–Nucleus Collisions

Shoji Nagamiya

Nuclear Science Division, Lawrence Berkeley Laboratory,
University of California, Berkeley, California 94720, U. S. A.
and
Department of Physics, Faculty of Science,
University of Tokyo, Hongo, Bunkyo-ku, Tokyo, Japan

Abstract

Experimental studies on particle correlations in proton-nucleus and nucleus-nucleus collisions at beam energies of 1 - 2 A·GeV are reviewed. Data are categorized into two types. One is those which provide fundamental information on the basic reaction mechanism. For example, the nucleon mean free path, the interaction radius, the fraction of the direct knock-out component, the pion-to-proton ratio, and the role of cluster in backward proton emission have been studied. The other is the data that have not yet been explained within the framework of orthodox theories. Hints of hydrodynamical flows are observed in these data. Finally, future experimental possibilities are discussed.

The work was supported by the Director, Office of Energy Research, Division of Nuclear Physics of the Office of High Energy and Nuclear Physics of the U.S. Department of Energy under Contract W-7405-ENG-48. It was also supported by the INS-LBL Collaboration Program.

INTRODUCTION

The research goal of high-energy nuclear collisions is to study the properties of highly excited, dense nuclear matter. With heavy-ion beams at $E_{\text{Beam}} \approx 1$ A·GeV we have a chance to compress nuclear matter to density higher than ρ_0 ($\simeq 0.17$ fm^{-3}) or to heat it to temperatures higher than the nucleon binding energy (16 MeV), whereas with elementary particle beams the creation of such hot, dense nuclear matter is not possible. So far, active experimental and theoretical studies toward this goal have been undertaken both at the Bevalac in Berkeley and at the Synchrophasotron in Dubna.

Actual experimental signals from high-energy nuclear collisions are, however, very complex. Fig. 1 shows a streamer chamber photograph from 1.8 A·GeV Ar + Pb collisions.[1] More than 50 charged-particle tracks are observed there. Immediately we notice that two major, important tasks are called for. The first task is to understand the basic reaction mechanism that determines various features of particle emission, such as energy and angular distributions, multiplicity, rate of particle production, projectile and target mass dependences, beam-energy dependence, etc. For this purpose inclusive data have been used extensively.[2–6] In spite of rich information contained in these inclusive data, it is rather obvious that the entire picture of high-energy nuclear collisions cannot be extracted from these data alone. In the presence of 50 charged particles, the single-particle inclusive data detect only a limited portion of the events. Clearly, measurements of particle correlations are needed. In this article we describe first to what extent we have understood the basic reaction mechanism from measurements of particle correlations.

The second important task is to extract new phenomena and/or new dynamical modes from the data. Here, it is important to ask whether the data contain significant deviations from what we normally expect from orthodox theories that describe the basic reaction mechanism. If deviations were detected, then we can ask how and why

these deviations are generated and how they are explained. During the last few years ambitious programs to search for such deviations have been developed from measurements of both inclusive spectra and particle correlations. In inclusive spectra the detection of subthreshold meson production,[7-11] superheavy fragment production,[12,13] or the particle production at around the absolute kinematical limit[14,15] has been tried, but no significant information on the new phenomena has been obtained. Two puzzles that have been explored so far in inclusive spectra are a too large entropy observed in the deuteron-to-proton ratio[16,6,17-21] and too short mean free paths of projectile fragments in emulsions.[22] These subjects have been reviewed elsewhere.[2,23] On the other hand, the data of particle correlations have shown hints of massive nucleon flows. In this article we discuss this last topic.

We also discuss proton-nucleus collisions. Since nucleus-nucleus collisions are so complex, the study of a much simpler system, proton + nucleus, often helps us to understand them. Specifically, the mechanism of backward proton emission in proton-nucleus collisions is discussed in this article, since it provides useful information on the mechanism of particle emission far beyond the free nucleon-nucleon kinematical limit in the nucleus-nucleus collision.

In Sec. 1 the measurements of (1) the mean free path (λ) of protons inside the nucleus and (2) the interaction radius (R) of the nucleus-nucleus collisions are described. These two macroscopic variables are the most basic quantities that determine the dynamics of nuclear collisions. In Sec. 2 the experimental evidence of the direct and multiple-collision processes is discussed. This study revealed the non-equilibrated nature of high-energy nuclear collisions. In Sec. 3 the data of multi-pion production are reviewed. The mechanism of secondary-particle emission has been clarified from these data. In Sec. 4 the data that have not been explained up to now are summarized and discussed. These data addressed the fundamental question of whether nuclei flow. It may be these data that will shed light on future studies of the physics of hot, dense nuclear matter. In Sec. 5 the current experimental efforts in the

study of particle emission into a kinematic region far beyond the free nucleon-nucleon kinematical limit are described, in both proton-nucleus and nucleus-nucleus collisions. Finally in Sec. 6 future possibilities and my personal opinions about the study of high-energy nuclear collisions are discussed.

1. MEAN FREE PATH (λ) AND INTERACTION RADIUS (R)

In nuclear collisions at beam energies of around 1 A·GeV the de Broglie wavelength of incident nucleons inside the projectile is about 0.3 fm (in the nucleon-nucleon c.m. frame) which is much shorter than the typical internucleon distance ($d \simeq 1.8$ fm). This fact implies that the projectile nucleons will recognize the individuality of target nucleons. Consequently, it is likely that individual nucleon-nucleon interactions, rather than the interactions through mean fields, determine the basic dynamics of high-energy nuclear collisions. In this case, the mean free path (λ) of nucleons inside the nucleus and the interaction radius (R) of nuclear collisions are the two important macroscopic quantities which determine the major feature of reaction dynamics. If $\lambda \gg R$, then each nucleon experiences at most one nucleon-nucleon (hereafter called NN) collision, and consequently the nuclear collision is described as a simple superposition of single NN collisions without any rescatterings. This is called the *direct* limit. On the other hand, if $\lambda \ll R$, then each nucleon experiences successive multiple collisions, and the available kinetic energy tends to be shared among all participating nucleons. This is called the ***thermal*** limit. Many theoretical models to describe either the direct[24-30] or the thermal[31-43] limit have been reported. In order to study the actual situation, however, it is very important to determine experimentally both the values of λ and R.

1.1. Determination of λ

First we describe recent measurements of two-proton correlations in proton-nucleus collisions.[44] The experimental layout is shown in Fig. 2. Four sets of detectors (called the U (up), D (down), R (right), and S) were prepared. Among these the first three are the plastic-scintillator telescopes which were placed at $\vartheta = 40°$ with respect to the beam direction. The last one, S, is the magnetic spectrometer. Although the spectrometer was rotatable from $\vartheta = 15°$ to 110°, the angle was fixed to 40° in this particular experiment. In azimuth the angular separation between two neighboring counters $\Delta\varphi$ was 90°. Integrated counts of protons with $E_p \geq 200$ MeV were measured by the three telescopes. On the other hand, the proton energy distribution in the energy region of 50 MeV $< E_p <$ 1 GeV was measured by the spectrometer.

Fig. 3 (a) shows inclusive proton spectra from p + C collisions at $E_{\text{Beam}} = 800$ MeV. A sharp peak is observed at forward angles (< 20°) primarily due to proton-proton (pp) or proton-neutron (pn) quasi-elastic scatterings. However, at large angles no peaks are observed. The 40° spectrum from the same reaction was studied in more detail from two-proton coincidences, as shown in Fig. 3 (b). If the coincidence between S and R (in-plane coincidence) was taken, the proton spectrum measured by S showed a very clean peak. At the peak the proton energy is about 400 MeV which is exactly what is expected from the pp quasi-elastic scattering process. On the other hand, no structures are observed for $S \cdot U$ or $S \cdot D$ (out-of-plane) coincidences.

Target-mass dependences of the yields due to quasi-elastic scatterings are plotted in Fig. 4. Fig. 4 (a) shows the mass dependence of inclusive yields at $\vartheta = 15°$ due to pp or pn quasi-elastic scatterings. These yields can be evaluated easily at forward angles, as a sharp peak is observed in the inclusive spectra (Fig. 3 (a)). The yields are proportional to A^α with $\alpha \approx 1/3$. Fig. 4 (b), on the other hand, shows the target-mass dependence of two-proton in-plane coincidence yields from pp quasi-elastic scatterings. The cross sections were evaluated from the in-plane-coincidence data at

40° from which were subtracted the out-of-plane coincidence data. For a light-mass target the cross section increases as the target mass increases. However, it reaches a maximum at $A \simeq 50$ and then in the region of $A > 50$ the cross section decreases as the target mass increases. This is because, although the probability of NN scatterings increases as the target mass increases, the probability of subsequent rescatterings increases as well. After the first collision, if either one of a pair of nucleons is rescattered, then the in-plane correlation vanishes.

By parameterizing the rescattering effect in terms of the proton mean free path, λ, the observed target-mass dependences were fitted. The best fit is obtained with λ = 2.4 fm (at 800 MeV and inside the $N = Z$ nucleus). If the value of λ was changed by 20 % from this value, then neither the observed shape nor the absolute value can be reproduced, as seen in Fig. 4 (b). Therefore, this method of two-proton coincidences is very useful for accurately determining the mean free path. The observed value of λ is slightly longer than the value expected from free NN collision, but is shorter than that obtained from the imaginary part of the optical potential.[45]

1.2. Determination of R

Next we discuss the determination of the interaction size from small-angle two-particle correlations. Suppose that two identical particles, such as two negative pions, are created at $(\vec{r},t) = (\vec{x}_1,t_1)$ and $(\vec{x}_2,t_2)$, and that these two particles are detected at $(\vec{X}_1,T_1)$ and $(\vec{X}_2,T_2)$. Then, within the plane-wave approximation, the observed two-particle spectrum is expressed as[46–52]

$$P(\vec{X}_1\ T_1,\ \vec{X}_2\ T_2) = \frac{1}{2}\ |\ \exp[i\vec{k}_1(\vec{X}_1-\vec{x}_1)-iE_1(T_1-t_1)]\cdot\exp[i\vec{k}_2(\vec{X}_2-\vec{x}_2)-iE_2(T_2-t_2)]$$
$$\pm\ \exp[i\vec{k}_1(\vec{X}_1-\vec{x}_2)-iE_1(T_1-t_2)]\cdot\exp[i\vec{k}_2(\vec{X}_2-\vec{x}_1)-iE_2(T_2-t_1)]\ |^2, \qquad (1)$$

where $(\vec{k}_i,E_i)$ are the momentum and energy of a particle detected at $(\vec{X}_i,T_i)$. The sign of $\pm$ corresponds to bosons (+) and fermions (-), respectively. The above equation can be rewritten as

$$P(\vec{X}_1\ T_1,\ \vec{X}_2\ T_2) = 1 \pm \cos[\vec{q}(\Delta\vec{x}) - E_0(\Delta t)], \tag{2}$$

with

$$\vec{q} = \vec{k}_1 - \vec{k}_2,\ \Delta\vec{x} = \vec{x}_1 - \vec{x}_2,\ E_0 = E_1 - E_2,\ \text{and}\ \Delta t = t_1 - t_2. \tag{3}$$

We first discuss two-pion emission such as $\pi^-\pi^-$; namely the case of a + sign in Eqs. (1) and (2). If the emitting source of pions has a space-time structure given by $\rho(\vec{r},t)$, then the actual two-pion spectrum, C_2, is given by

$$C_2 = \int P(\vec{X}_1\ T_1,\ \vec{X}_2\ T_2)\rho(\vec{x}_1,t_1)\rho(\vec{x}_2,t_2)d\vec{x}_1 d\vec{x}_2 dt_1 dt_2. \tag{4}$$

For example, in the case where

$$\rho(\vec{r},t) \propto e^{-r^2/R^2} \cdot e^{-t^2/\tau^2}, \tag{5}$$

we have[51]

$$C_2 = 1 + \exp[-|\vec{q}|^2R^2/2 - E_0^2\tau^2/2]. \tag{6}$$

Therefore, $C_2 = 1$ at $(|\vec{q}|, E_0) \to \infty$, and $= 2$ at $|\vec{q}| \to 0$ (in this case E_0 is automatically 0). The width of the shape of C_2 is characterized by R and τ. Namely, from the measurements of the above interference pattern, C_2, we can determine the source size (R) and the collision time (τ).

Eq. (1) assumes that two pions are emitted from two independent points without any coherence. If these two points are strongly correlated, such as seen in a pion lazer, then such an interference pattern disappears.[52] The peak height of the interference pattern, C_2, may thus tell us the degree of coherence in the pion production.

The measurement of C_2 was first performed experimentally in a streamer chamber from $2\pi^-$ detection with 1.8 A·GeV Ar beams.[53] Since this experiment a large number of data of pion interferometry have been collected.[54–56] Here, recent data by Zajc *et al.*[56] are discussed. The data are shown in Fig. 5. Zajc *et al.* have generalized Eq. (6) to

$$C_2 = 1 + \alpha \exp[-|\vec{q}|^2 R^2/2 - E_0^2 \tau^2/2], \qquad (6')$$

so that one can take into account the coherence effect by introducing the parameter α. We must note that actual two-pion spectra are largely affected by the final state interactions. These interactions originate both from Coulomb and strong interactions, and especially from the former because $\pi^-\pi^-$ ($T = 2$) strong interactions at small relative momentum are negligibly small. If we apply a standard Gamov correction for Coulomb interactions, then two-pion spectra are significantly changed, as shown in Fig. 5. Therefore, the widths for the raw data do not immediately reflect R and τ. The data were first analyzed by fixing α to 1 (upper graphs in Fig. 5). After the Coulomb corrections the value of $R = 3.0 \pm 0.3$ was obtained for a 1.8 A·GeV Ar + KCl system. The value of R is largely unchanged when α is left as a free parameter (lower graphs in Fig. 5). A slight deviation of α from 1 may indicate the existence of coherence of pion production, but at the present moment it is too early to conclude anything definite on this point.

It might be worthwhile to mention here the data for two-proton interferometry. In this case the correlation function, C_2, becomes 0 at $|\vec{q}| = 0$, because of the - sign for fermions in Eqs. (1) and (2). Zarbakhsh *et al.*[57] have recently measured C_2 for two protons in 1.8 A·GeV Ar + KCl collisions, as shown in Fig. 6. The observed correlation function shows a peak at $|\vec{q}| \simeq 20$ MeV/c. In this case both repulsive Coulomb and attractive strong interactions are important. The strong interaction induces a positive correlation while the Coulomb interaction induces a negative correlation, and the net correlation pattern creates a peak at a certain momentum.[50] In this experiment, a smaller source radius is observed for proton emission at $y = (y_P+y_T)/2$ than at $y = y_P$, where y_P and y_T are the projectile and target rapidities, respectively. In addition, a much smaller radius is obtained for higher-multiplicity events. This last statement is not consistent with the recent result of two-pion interferometry.[55] Although the radius obtained by two-proton interferometry is generally smaller than that obtained by two-

pion interferometry, it may again be too early to conclude something definite from these analyses, mainly because of the complex nature of the final state interactions.

1.3. Implication of the Data

From the above two measurements we ascertain that $\lambda \simeq 2.4$ fm and $R \simeq 3$ fm. Namely, $\lambda \simeq R$. Therefore, both direct and thermal limits are unrealistic. The actual collision process is just in between these two limits. Here we find one of the complexities of the reaction mechanism of high-energy nuclear collisions.

2. EVIDENCE OF DIRECT AND MULTTIPLE–COLLISION PROCESSES

Under the condition that $\lambda \simeq R$ it is interesting to know quantitatively the relative importance of the direct and the thermal components in nuclear collisions. This question has been investigated using large-angle two-proton correlations. We show the data for 800 A·MeV C + C collisions.[58–61] The experimental arrangement was the same as that shown in Fig. 2. Consider the ratio, C, defined by

$$C \equiv \frac{2 \times S \cdot R}{S \cdot U + S \cdot D}, \tag{7}$$

where $S \cdot R$ indicates the coincidence counts between the spectrometer (S) and the R-telescope. This ratio is a measure of coplanarity. If the thermal process were dominant, the ratio C would be close to one, because there particle emission tends to be statistical. On the other hand, if only the direct process were important, this ratio would be larger than one, because *pp* quasi-elastic scatterings induce two-proton emission in the same reaction plane. In 800 A·MeV C + C collisions the observed ratio, C, is larger than one, as shown in Fig. 7, and it has a peak at the exact momentum which is expected from *pp* quasi-elastic scatterings. Therefore, this experiment clearly demonstrates the importance of the direct process.

However, the data of Fig. 7 also show a strong evidence of the existence of multiple *NN* collisions. If all protons are emitted from direct processes only, then the calculated peak height of $(C - 1)$ must be about six times larger than the observed one. This fact implies that the coplanar two-proton correlations are somewhat diluted by the existence of multiple *NN* collisions. If one of two protons from a *pp* quasi-elastic scattering is rescattered after this first collision, then the coplanar correlation vanishes. Therefore, the probability that one nucleon experiences the first collision only is roughly given by $\sqrt{1/6} \simeq 0.4$, where $1/6$ is the dilution factor of the peak height of $(C - 1)$. In other words, the probability for each nucleon to experience multiple *NN* collisions is about 0.6 in 800 A·MeV C + C collisions. This number is consistent with various recent theoretical predictions.[62–65]

It is expected that the contribution from the direct process would be suppressed when high-multiplicity events were selected. In fact, it is shown[66] that the proton angular distribution in the c.m. frame approaches isotropy for higher-multiplicity events, reflecting less of a contribution from the direct process. From the comparison between high-event-multiplicity data and inclusive data, the fraction of the direct component was thus evaluated. It is shown in Ref. 66 that the fraction of the direct component is about 0.4 for small proton energies at $E_p^{\text{c.m.}} \simeq E_{\text{Beam}}^{\text{c.m.}} / A$, which is consistent with the above two-proton correlation data. On the other hand, this fraction decreases substantially as the energy of the emitted proton increases.

It is also expected that the contribution from the direct process will be suppressed more as the projectile and target masses increase. Reflecting this expectation, evidence of *pp* quasi-elastic scatterings has not been observed in a system heavier than Ar + Ar. For instance, in Ar + Pb collisions, two-proton correlations exhibit a completely different pattern, as we will discuss later in Sec. 4.

3. MULTI-PION PRODUCTION

Multi-pion production has recently been measured in a streamer chamber for 1.8 A·GeV Ar + KCl[67] and Ar + Pb[55] collisions. For example, in the case of Ar + Pb the observed pion multiplicity per event extends up to 19. In this paper, the multiplicity correlation between pions (m_π) and charged nuclear fragments (m_Z) is discussed.

Naively one would expect that m_π increases as m_Z increases. In a streamer chamber it is easy to identify negatively charged tracks which are mostly from π^-. Positively charged tracks contain both π^+ and nuclear fragments. For nearly equal-mass collisions with $Z \simeq A/2$ we expect $m_{\pi^-} \simeq m_{\pi^+}$. Therefore, to a good approximation, the difference in numbers between positively and negatively charged tracks is nearly equal to m_Z. In Fig. 8 (a) the multiplicity correlation between m_π and m_Z is plotted for 1.8 A·GeV Ar + KCl collisions. We observe a strong linear correlation between them.[67] A similar study has been done for 1.8 A·GeV Ar + Pb.[55] In this case we cannot assume $m_{\pi^-} \simeq m_{\pi^+}$, since $N \neq Z$. Therefore, plotted in Fig. 8 (b) is the multiplicity correlation between π^- and the total charged particles (which include both positively and negatively charged particles). No linear correlation is observed for Ar + Pb. In addition, for $m_{\pi^-} \geq 10$, the total event multiplicity stays almost constant in spite of the fact that the value of m_{π^-} yet increases. Furthermore, for $m_{\pi^-} = 0$ a finite number of charged particles are observed. So far, these phenomena for Ar + Pb have not been well understood.

In connection with the above study we cite the data of the projectile- and target-mass dependence of $\langle m_\pi \rangle$ obtained from inclusive data. Plotted in Fig. 9 are the observed values of $\langle m_\pi \rangle$ as a function of the average participant nucleon number, P, for various projectile and target combinations at E_{Beam} = 800 A·MeV.[6] Here the value of P was evaluated from the participant-spectator model,[68] and is expressed as[69,70]

$$P = \frac{A_P A_T^{2/3} + A_T A_P^{2/3}}{(A_P^{1/3} + A_T^{1/3})^2}, \quad (8)$$

where A_P and A_T are the projectile and target mass numbers, respectively. The observed values of $\langle m_\pi \rangle$ are roughly parametererized as[2]

$$\langle m_\pi \rangle = a \cdot P^x, \quad (9)$$

with $x \simeq 2/3$. This implies that the pions are emitted from the surface of the participant region. It seems that this fact is inconsistent with what we have learned from Fig. 8 (a), since there the almost linear correlation between m_π and m_Z is observed. However, we should note that the data of Fig. 9 can be fitted with $x \simeq 1$ if the data are limited to only light-mass combinations up to Ar + KCl. The value of $x \simeq 2/3$ is obtained when the data are extended to a region of heavier masses up to Ar + Pb. The $P^{2/3}$ dependence of $\langle m_\pi \rangle$ suggests the importance of the pion absorption process. Of course, from these data alone we cannot conclude whether the pion is absorbed in the participant region or in the spectator region. But, it is almost certain that all theoretical models need to include this absorption effect.

According to the participant-spectator model, the value of m_Z is directly related to the impact parameter, since the participant nucleon number is related uniquely to the collision geometry. Thus, it seems possible to measure the distribution of m_π at a fixed impact parameter. An example of such a study is shown in Fig. 10. Here, events with $m_Z \geq 30$ were selected for Ar + KCl collisions in a streamer chamber.[67] Since the maximum value of m_Z is 36 in this case, the collision is almost head-on; the corresponding maximum impact parameter, b_{max}, is about 2.2 fm. The observed distribution is of a Poisson type which has been expected on very general theoretical grounds.[71] In this Poisson distribution the square of dispersion, D^2, must be proportional to the average multiplicity, $\langle m_\pi \rangle$. The linear relation between D^2 and $\langle m_\pi \rangle$ was confirmed for various values of m_Z in Ar + KCl collisions.[67]

4. HINTS OF MASSIVE NUCLEON FLOWS

In the presence of frequent multiple *NN* collisions a macroscopic aspect of high-energy nuclear collisions might show up. This could be, for example, massive nucleon flow, compression, or explosion. In order for such a macroscopic motion to occur, the mean free path of nucleons (λ) must be much shorter than the size of the interaction region (R); namely $\lambda \ll R$. However, we learn from Sec. 1 that $\lambda \simeq R$ at beam energies around 1 A·GeV, at least for a light-mass nuclear system. Therefore, we have to make either R longer or λ shorter. Since the total nucleon-nucleon cross section is almost independent of the beam energy, the value of λ is nearly uncontrollable. On the other hand, we can make the value of R longer by increasing the participant nucleon number. Obviously the use of heavy-mass projectiles and targets is effective for this purpose. In addition, the selection of small impact parameter is useful. In the small impact parameter the nuclear collision tends to be violent, and the event multiplicity tends to be high. Therefore, high-multiplicity events have been selected and studied for the heavy-mass nuclear system.

There are two methods to select high-multiplicity events. The first method, which is the most straightforward one, is the detection of as many particles as possible using a large number of counter arrays which surround the target.[72,66] The other method, which is suitable for low-intensity beams of $\leq 10^{(5-6)}$ projectiles/sec, is the selection of as few high-Z particles as possible at 0° downstream of the target,[73,67] where Z is the charge of the fragment. The reason for this is that high-multiplicity events tend to spray nuclear charge over a wide range of angles by leaving a small fraction of charge at 0°.

In this article four pieces of data of particle correlations, which seem to provide hints of massive nucleon flows, are described. The first example is the high-multiplicity events in nuclear emulsions. Baumgardt *et al.*[74] showed that the angular distribution of α particles peaks at a certain angle which is expected from nuclear shockwaves.[75] A

similar trial was repeated later by Heckman *et al.*[76] who, however, found less evidence of this peaking. Experimentally this interesting problem still remains an open question and further tests are needed especially from counter experiments.

The second hint is seen in a broad sideward peak observed in 393 A·MeV Ne + U collisions.[72] As shown in Fig. 11, the proton spectra show a forward peaking for low-multiplicity events. However, in high-multiplicity events the forward emission is highly suppressed. In addition, for very low-energy protons [$p_p \simeq 150$ MeV/c ($E_p \simeq 12$ MeV)], a broad peak is observed at $\vartheta_{\rm Lab} \simeq (70-90)°$. Stöcker *et al.*[77,78] have recently interpreted this broad peaking as due to the effect of the side splash of collective nucleon flow, as illustrated in Fig. 12 (a). At small impact parameters in Ne + U collisions a large body of the target nucleus is pushed forward by the projectile nucleus, especially in the overlapped region between the projectile and target. In the non-overlapped region, however, the nuclear matter will not receive such a forward push. Instead, it is likely to be pushed sideward. This sideward splash is expected in the low-energy region of fragments, since this non-overlapped region is mainly the spectator. In Ref. 78 it is further pointed out that calculations other than the hydrodynamical model,[79,80] such as the cascade,[81,82] thermal,[37] and thermal-plus-direct[83,84] models, do not predict a sideward peak.

The third hint for the massive nucleon flow is seen in the data of two-proton correlations in 800 A·MeV C + Pb or Ar + Pb collisions.[61,85,86] The experimental layout is the same as that shown in Fig. 2. The ratio C defined by Eq. (7) was measured as a function of the angle and energy of the protons detected by the spectrometer, S. Since high-energy protons with $E_p \geq 200$ MeV were selected by the three telescopes placed at $\vartheta_{\rm Lab} = 40°$, we call these protons the *fast* protons. The spectrometer, on the other hand, was rotated at angles from 15° to 110° and detected both low- and high-energy protons above 50 MeV (namely, both *slow* and *fast* protons). The implication of the ratio C is as follows: If $C > 1$, then two protons tend to be emitted on opposite sides in azimuth, while if $C < 1$, then they tend to be emitted on the same side.

Contour lines of the observed C are plotted in Fig. 13. At $(\vartheta, E) \simeq (40°, 1\ \text{GeV})$ we have $C < 1$. This implies that, once the first *fast* proton was detected by one of the telescopes at 40°, then the second *fast* proton tends to be emitted on the same side at $\vartheta \simeq 40°$, as illustrated in Fig. 14 (left). On the other hand, at $(\vartheta, E) \simeq (90°, 30\ \text{MeV})$ we observe $C > 1$. In this case, if the first *fast* proton was detected at 40°, the second *slow* proton is emitted on the opposite side at 90°, as illustrated in Fig. 14 (right). These features are exactly what we expect from the bounce-off effect of the hydrodynamical flow,[77,85,86] as shown in Fig. 12 (b), since the projectile "chunk" induces fast-fast correlation on the same side, whereas the projectile and target "chunks" induce fast-slow correlation on the opposite side.

The last hint of the massive flow is obtained from the energy spectra of protons and pions for high-multiplicity events.[66] Data are shown in Fig. 15 in which the observed energy spectra at 90° in the c.m. frame are plotted for 800 A·MeV Ar + KCl collisions. Typical features are (1) the non-exponential shape for protons, (2) the exponential shape for pions, and (3) the steeper slope for pions than for protons. Although the "shoulder-arm" type energy distribution for protons is already observed in the inclusive spectra,[6] the flattening of the shape in the low-energy region as well as the difference in exponential slopes between protons and pions are more pronounced in high-multiplicity events. In the phase-space model the "shoulder-arm" feature has been thought of as due to the existence of NN quasi-elastic scatterings,[87] since these scatterings increase the proton yield at $E_p^{\text{c.m.}} \simeq E_{\text{Beam}}^{\text{c.m.}}/A$ (= 182 MeV in this case). In high-multiplicity events these NN quasi-elastic components are expected to be suppressed. Still, the "shoulder-arm" shape remains. In order to solve this puzzle, Siemens and Rasmussen[88] proposed a radially exploding nucleon flow. At a fixed kinetic energy the velocity of a proton is much smaller than that of a pion. Therefore, if there is an explosive flow, then it introduces more of an enhancement of kinetic energy for protons than for pions. Consequently, the proton spectra become broader than the pion spectra. The best fit to the data by this model is shown in Fig. 15.

Although the absolute yields of pions are underestimated by this model,[89] the observed shapes for both protons and pions are reasonably well reproduced.

Currently the discussions of hydrodynamical effects are still weak and somewhat speculative. Theoretically, the basic assumption involved in the hydrodynamical model, i.e., $\lambda \ll R$, is not well justified even after the selection of high-multiplicity events, since the largest value of R obtainable is 5 - 6 fm, whereas λ = 2 - 3 fm. Experimentally, the hydrodynamical effects shown here are only 10-30 % effects compared to the normal statistical backgrounds. Obviously more work is needed. In spite of these shortcomings, we point out here that future efforts to search for massive nucleon flows are extremely important and interesting, since they might reveal new phenomena in high-energy nuclear collisions. Let us wait and hope for U + U collisions.

5. PARTICLE EMISSION FAR BEYOND FREE NUCLEON–NUCLEON KINEMATICS

One of the unique features of nuclear beams or nuclear targets is particle emission into a kinematic domain far beyond the free *NN* kinematical limit. In this article we discuss mainly the mechanism by which protons are emitted into such a kinematic domain.

5.1. High-p_T Proton Emission in Nucleus–Nucleus Collisions

First we study the production of high-p_T protons in nucleus-nucleus collisions. Proton spectra in almost equal-mass nuclear collisions (A + A) has been measured at c.m. 90° at a beam energy of 800 A·MeV in the region of A = 12 - 40.[6] The observed cross section can be parameterized, to a good approximation, as

$$E\,\frac{d^3\sigma}{d^3p} \propto A^{\alpha}, \tag{10}$$

where A is the projectile (and target) mass. Experimental values of α are displayed in Fig. 16 for various c.m. kinetic energies, $E_p^{\text{c.m.}}$. In the low-energy region below the free

NN kinematical limit (in this case, 182 MeV), the value of α is very close to the geometrical limit of 5/3; in this limit the cross section is proportional to the product of the participating nucleon number ($\propto A$) times the geometrical cross section ($\propto A^{2/3}$). However, in the high energy region the power α exceeds 2 and finally reaches the value of 2.6 or 2.7 at the highest energy observed in this experiment. Such a large value of α strongly suggests that multiple *NN* collisions are important for the creation of these high-energy (in this case high-p_T) protons.

An extreme limit of the multiple collision is the thermal process. However, in the thermal limit the power α becomes again the geometrical limit of 5/3.[90] Therefore, the observed power dependence indicates that, although high-energy protons are created from multiple *NN* collisions, they are not extremely frequent multiple collisions. Then, an immediate question is how many nucleons are actually involved. This question has been studied by many theorists.[87,90,91] According to a recent calculation,[90] the average number of *NN* collisions, $<n>$, monotonically increases as the observed proton energy increases. The value of $<n> \simeq 3$ for $E_p^{c.m.} \approx 200$ MeV and $\approx$ 4-5 for $E_p^{c.m.} \approx 800$ MeV for the Ar + KCl system.

It is interesting to study experimentally in more detail the creation mechanism of high-p_T protons by means of particle correlations. This program is currently in progress in Berkeley.[92] As shown in Fig. 17, a region of very high *energy* density must be created in order to produce very high-p_T protons. We conventionally call this region the local hot spot. Suppose that the volume of this local hot spot is small (< 1 fm^3). Then, we have the following situation: that, if a very high-energy proton is emitted in a certain direction, then low-energy nucleons are emitted in the opposite direction, compensating for the momentum of the first high-energy proton by a large number of recoil nucleons. In the absolute kinematical limit this mechanism is responsible, and it is called the *recoil-like* correlation. On the other hand, suppose that the volume of the local hot spot is relatively large (over a region of a few nucleons). Then, if a high-energy proton is emitted in a certain direction, then again high-energy nucleons are

emitted in the opposite direction. This is called the *jet-like* correlation. Whether the recoil-like or jet-like mechanism is responsible for high-p_T proton emission is an interesting question, and this question is currently being tested with a large experimental device installed inside a 2-meter-diameter magnet called HISS.

5.2. Backward Proton Emission in Proton–Nucleus Collisions

A clean example of proton emission far beyond the free *NN* kinematical limit is also seen in proton emission at backward angles in proton-nucleus collisions.[93–99] Thus far, two competing mechanisms have been proposed for the creation mechanism, as illustrated in Fig. 18. The first one, which was proposed by Frankel[93] and Amado and Woloshyn,[94] is that high-momentum tails of the nucleon Fermi motion inside the target produce backward protons. This is similar to shaking a coffee cup so that the contents are spilled out in a backward direction. However, in order to explain the observed backward spectra the exponential type Fermi momentum distribution, $\exp(-k/k_0)$ with $k_0 \simeq 90$ MeV/c, has to be assumed.[93] Because the origin of the exponential shape is uncertain, the other mechanism was also proposed. In this it is assumed that a cluster is formed inside the target nucleus, and thereby, the incident proton can be kicked out by this cluster into the backward direction, as illustrated in Fig. 18. Here the cluster is called the fluctuon by the Dubna group[95,96] or the correlated cluster by Fujita *et al.*[97,98]

Are these two competing mechanisms the same or different? Since the second mechanism requires short-range correlations between nucleons to create a cluster, and since the Fourier transform of these correlations produces high-momentum tails in the momentum space, it seems that these two mechanisms are correlated. However, from the particle correlation measurements the first mechanism can be kinematically separable from the second. If we write down symbolically the process of backward proton emission as

$$p + nN \rightarrow \text{(backward proton)}, \qquad (11)$$

where nN indicates n-nucleon cluster, then the first mechanism corresponds to $n = 1$, whereas the second mechanism corresponds to $n \geq 2$. We now detect two protons, one at a backward angle and the other at a forward angle. In a momentum-momentum scatter plot between the two protons, as shown in Fig. 19 (left), we can draw a line (the solid line) along which $E_B + E_F \simeq E_{Beam}$, where B and F refer to backward and forward, respectively. This line indicates that the two protons originate from pp quasi-elastic scatterings, and thus from the $n = 1$ process only. On the other hand, in the kinematic domain inside this line two protons can come from the process with $n \geq 2$, since in this process the available energy is shared among more than two nucleons, and therefore $E_B + E_F < E_{Beam}$. For example, if a backward proton were emitted from a $p + d$ collision followed by the break-up of this d-cluster into $p + n$, then the sum of two proton energies would be approximately $E_{Beam}/2$, as indicated by the dashed line in Fig. 19. If a backward proton were detected in coincidence with a forward deuteron under the condition of $E_B + E_F \simeq E_{Beam}$, then the $n = 2$ process would be selected, as illustrated in Fig. 19.

Based on this idea Komorov *et al.*[99] measured forward-backward coincidences. Since a recent experiment in Berkeley involving pp and pd coincidences[100] covers a much wider kinematic region than the experiment by Komorov *et al.*, we discuss these new results here. In this experiment 22 sets of counter telescopes together with a magnetic spectrometer were prepared. As a subset of this system two sets of ΔE-E telescopes and a magnetic spectrometer are shown in Fig. 20. These counters were named BI, BO, and S, and were placed at $(\vartheta,\varphi) = (118°,180°)$, $(118°,90°)$ and $(15°,0°)$, respectively. Coincidences of $BI \cdot S$ (in-plane) and $BO \cdot S$ (out-of-plane) were measured.

In Fig. 21 the momentum-momentum scatter plots between two counters S and BI (in-plane coincidences) are displayed. Here, at $\vartheta = 118°$ only protons were detected by BI, whereas at $\vartheta = 15°$ both protons and deuterons were detected by S. In the pp

and *pd* quasi-elastic scattering processes, once the first proton was detected by *BI*, then the second proton or deuteron would be emitted at a certain preferential angle. The angle 15° is perfectly suitable for detecting *pd* quasi-elastic scatterings but about 5° off from the most preferred angle *pp* quasi-elastic scatterings. Nevertheless, the contributions from both *pp* and *pd* quasi-elastic scatterings are clearly observed, as indicated by the solid lines in Fig. 21. We therefore learn that both the n = 1 and 2 processes seem to contribute to the backward proton emission. From the *pp*-coincidence data we also learn that some protons are emitted from the break-up of deuterons, or possibly of heavier fragments (see the dashed lines in Fig. 21).

Quantitatively, how much is from n = 1 and how much is from n = 2? To answer to this question, a rather careful study of kinematics and detector solid angles is required. Although no solid conclusions have so far been obtained on this point, we discuss the preliminary results. In Fig. 22 the backward proton spectra under several coincidence conditions are displayed. In *pp* coincidences QES indicates the *pp* quasi-elastic scattering component obtained from the $BI \cdot S$ in-plane coincidence, NON-QES indicates the non-*pp*-quasi-elastic component but from the in-plane coincidence, and OUT-OF-PLANE indicates the contribution from the $BO \cdot S$ out-of-plane coincidence. The slope is the steepest for OUT-OF-PLANE. Also, the slope for QES is steeper than that for NON-QES. The slope for the inclusive spectra is close to the case of this NON-QES. Therefore, we learn that the n = 1 process (primarily contributing to QES) as well as the large n process (primarily contributing to OUT-OF-PLANE) are not important for high-energy proton production. The NON-QES ($n \geq 1$ but not large) seems to contribute most to the production of high-energy backward protons. In *pd* coincidences, as shown in Fig. 22 (b), both QES (n = 2) and NON-QES ($n \geq 2$) contribute to this backward production, while OUT-OF-PLANE (n: large) does not. From these studies we learn that high-energy backward protons are mainly from processes with $n \geq 2$ and not from those with n = 1 nor from those with large n. In other words, the second mechanism in Fig. 18 seems more important than the first for the production of

high-energy backward protons.

Another interesting aspect of the *pp* coincidence in proton-nucleus collisions is the possibility of determining the shape of Fermi motion up to a momentum of about 500 MeV/c. In particular, the *pp* quasi-elastic scattering data are the most useful, since these data select the process of binary *pp* collision, one from the projectile and the other from the target. For example, *pp* quasi-elastic scatterings are observed even at $\vartheta_1 = \vartheta_2 = 20°$ in 800 MeV *p* + KCl collisions.[101] Such an observation is possible only when a proton inside the nucleus carries the Fermi momentum of $\geq$ 330 MeV/c. Whether or not the shape of Fermi motion deviates greatly from a Gaussian shape in the high momentum region is a very interesting question. In the future, the (*p*,2*p*) experiment incorporated with the (e,e'*p*) experiment will clarify the structure of high-momentum tails more than in the past.

6. FUTURE POSSIBILITIES

So far, I have discussed mainly the existing data of particle correlations and their implications and explanations. What can we learn in the future? Here, I will discuss two interesting subjects, and at the end I discuss also the experiments needed in the future.

6.1. Multi-Baryonic Excited States

The first topic is the creation of multi-baryonic excited states. So far, the main research goal of high-energy nuclear collisions has been the search for new exotic phases such as abnormal nuclear matter,[102-104] pion condensation,[105-108] shockwaves,[109] and pionization[110,111] associated with high density nuclear matter, as shown in Fig. 23. However, two difficulties in creating such an exotic phase may exist. The first one is related to time dependence. According to a recent calculation by Gudima and Toneev,[112] density greater than $3\rho_0$ can actually be created with nuclear

collisions but only for a time interval of the order of $(2 - 3) \times 10^{-23}$ sec, as shown in Fig. 24. We must note that new exotic phases were predicted only for *static* high-density nuclear matter. In order for the system to change into such exotic phases, a certain relaxation time is required. The minimum relaxation time is of the order of 10^{-23} sec ($\approx R/c$) which is already comparable to the time interval during which the system is at its high-density phase. Thus, the system may not have enough time to undergo the phase transition into exotic phases. Here we find the first difficulty.

The second difficulty is related to the dynamical path. In order to create high-density nuclear matter, a large fraction of available energies must be converted into massive compression energy; namely the dynamical path A in Fig. 23. However, in actual nuclear collisions, these energies might be used only for exciting nucleons into baryonic excited states such as Δ, N^*, or Λ, without compressing nuclear matter; namely the dynamical path B. Under such circumstances what should we pursue in the future?

One promising subject in this case will be the study of multibaryonic excited states. For example, a multi Δ system is one interesting subject. At beam energies of around 700 A·MeV at which the production cross section of Δ reaches its maximum, each nucleon-nucleon collision creates Δ at a probability of about 50 %. In U + U collision we have about 60 NN collisions as an average. Therefore, about 30 Δ-particles are created. Since these Δ-particles are almost at rest in the NN c.m. frame, and since they are created within a radius of a few fm, they have a strong chance to interact with each other to form a Δ-soup[113–115] (see Fig. 25). Perhaps a meta-stable $^{16}\Delta$ might exist,[116] since there all spin-isospin sublevels are occupied in the 1s orbit. Perhaps, the high-density phase is expected in the Δ soup.[114,115] The search for such an exotic nucleus is an interesting challenge for the future.

If we use light nuclei as projectiles, the study of dibaryons ($\Delta\Delta$, $\Lambda\Lambda$, etc.) may also be interesting. So far, experimental searches for dibaryons have been done mostly

with elementary-particle beams such as γ, p, K, etc.[117] Nuclear beams, however, may offer a unique opportunity for this study. Whether a $\Delta\Delta$ system is tightly bound,[118-122] or whether a $\Lambda\Lambda$ system forms a meta-stable state[123] are very interesting questions.

6.2. Applications of Neutron-Rich Isotopes

The second subject is the use of neutron-rich isotopes. In a nucleus-nucleus collision, some of the projectile nucleons experience hard NN collisions with target nucleons, while other remainder nucleons do not. These remainder nucleons are called the spectator, and they eventually form projectile fragments. These fragments tend to keep various properties that the projectile nucleus had before the collision. For example, they have almost the same velocity as the beam velocity.[3] With regard to the neutron-to-proton (N/Z) ratio, the heavy-mass projectile such as U contains more neutrons than protons ($N/Z \approx 1.6$ for U). On the other hand, it is well known that the stability line of nuclei extends along $N/Z \approx 1$ for light nuclei. Therefore, light-mass projectile fragments from U beams tend to fill the unstable neutron-rich region.

Based on this idea Symons *et al.*[124] and Westfall *et al.*[125] have accelerated ^{40}Ar ($N/Z \simeq 1.2$) and ^{48}Ca ($N/Z \simeq 1.4$) beams and discovered 16 new isotopes in the projectile fragments especially from the latter. This type of study may open up a variety of applications of high-energy nuclear collisions, especially when U beams become available. Is there a new region of stability? How about a new region of deformation? Is the proton radius significantly different from the neutron radius? How about the static properties of new isotopes, such as lifetimes or magnetic moments? We can raise many questions.

One interesting application of these isotopes is their use as secondary beams. Since velocities of these isotopes are almost equal to the beam velocity, high-quality secondary beams are expected. For example, the use of an internal target to extract neutron-rich beams would be possible. Also, the preparation of a storage ring, as shown in Fig. 26 may help to extract neutron-rich beams. So far, only stable nuclei

have been used as projectiles. With the use of the internal target or storage ring, it may not be just a dream to have unstable neutron-rich nuclei such as ^{52}Ca as projectiles.

6.3. Needed Experimental Tasks

In summary, we list the following future programs:

First, we must solve the current puzzles. As mentioned in Sec. 4, we have observed hints of shockwaves, massive nucleon flows, and explosion. In addition, the projectile fragments with anomalously short mean free paths inside emulsions (called anomalon)[22] have been discovered. These current puzzles have to be reexamined experimentally in the immediate future.

Secondly, a 4π-solid-angle experiment is needed in the future particle correlation studies. A unique facility toward this goal has recently been fabricated in Berkeley, which is called the plastic ball-wall.[126] In Saclay, the 4π detector, called the DIOGENE, is under construction.[127] A streamer chamber is also very useful. A digital readout of this chamber is an interesting project.[128] For the analysis of the 4π data, global quantities such as "thrust",[129-131] "sphericity",[132] or "centrality",[133] etc. might be useful.

Thirdly, the measurements of extremely small cross sections are interesting. The smallest cross section measured so far is of the order of 1 $(\mu b \cdot GeV)/(sr \cdot (GeV/c)^3)$. However, new phenomena might be hiding at the level of much smaller cross sections. With current accelerator and detector technology, it is possible to measure the cross section down to 1 $(nb \cdot GeV)/(sr \cdot (GeV/c)^3)$ and perhaps down to 1 $(pb \cdot GeV)/(sr \cdot (GeV/c)^3)$. Obviously, a special experimental device is needed to measure such low cross sections. For example, a large magnet system called HISS[134] developed in Berkeley might be useful.

In the fourth, the measurements of new physical quantities or particles that have never been measured would be interesting. What we can handle now are the energy

and angular distributions of nuclear fragments, pions, kaons, and lambdas. However, other kinematic variables might have to be measured in the future. They are, for example, angular momentum, spin, polarization, delayed coincidence, etc. Also, particles such as γ-rays, leptons, or lepton pairs might have to be detected. These particles are especially important for the study of the initial violent stage.

In the fifth, the application of neutron-rich isotopes is again emphasized. In the sixth, the possibilities of studying multi-baryonic excited states are again repeated. These last two topics might form highlights of high-energy nuclear collisions in the coming few years.

ACKNOWLEDGMENTS

Stimulating discussions with M. Gyulassy, I. Tanihata, Y. Miake, and W. Zajc are gratefully acknowledged. Also, the help by Jeanne Miller to complete the manuscript is appreciated. This work was supported by the Director, Office of Energy Research, Division of Nuclear Physics of the Office of High Energy and Nuclear Physics of the U.S. Department of Energy under Contract W-7405-ENG-48. It was also supported by the INS-LBL Collaboration Program.

References

1. This streamer-chamber photograph was taken at the Bevalac by the group of the Univeristy of California at Riverside.
2. S. Nagamiya, in Proceedings of the 5th High Energy Heavy Ion Summer Study, LBL-12652, Conf-8105104, Berkeley, May, 1981, p.141.
3. D. E. Greiner, P. J. Lindstrom, H. H. Heckman, B. Cork, and F. S. Bieser, Phys. Rev. Lett. 35, 152 (1974).
4. J. Papp, J. Jaros, L. Schroeder, J. Staples, H. Steiner, A. Wagner, and J. Wiss, Phys. Rev. Lett. 34, 601 (1975).
5. A. Sandoval, H. H. Gutbrod, W. G. Meyer, R. Stock, Ch. Lukner, A. M. Poskanzer, J. Gosset, J.-C. Jourdain, C. H. King, G. King, Nguyen Van Sen, G. D. Westfall, and K. L. Wolf, Phys. Rev. C21, 1321 (1980).
6. S. Nagamiya, M.-C. Lemaire, E. Moeller, S. Schnetzer, G. Shapiro, H. Steiner, and I. Tanihata, Phys. Rev. C24, 971 (1981).
7. W. Benenson, G. Bertsch, G. M. Crawley, E. Kashy, J. A. Nolen, Jr., H. Bowman, J. G. Ingersoll, J. O. Rasmussen, J. Sullivan, M. Koike, J. Peter, and T. E. Ward, Phys. Rev. Lett. 43, 683 (1979); Phys. Rev. Lett. 44, 54 (1980) (E).
8. S. Nagamiya, H. Hamagaki, P. Hecking, R. Lombard, Y. Miake, E. Moeller, S. Schnetzer, H. Steiner, S. Kadota, I. Tanihata, S. Bohrmann, and J. Knoll, preprint (1982).
9. S. Schnetzer, Thesis, Lawrence Berkeley Laboratory Report LBL-13727 (1981), unpublished.
10. J. W. Harris, A. Sandoval, R. Stock, H. Stroebele, R. E. Renfordt, J. V. Geaga, H. G. Pugh, L. S. Schroeder, K. L. Wolf, and A. Dacal, Phys. Rev. Lett. 47, 229 (1981).
11. A. Shor, K. Ganzer, J. Carroll, G. Igo, J. Geaga, S. Abachi, A. Sagle, T. Mulera, V. Perez-Mendez, P. Lindstrom, F. Zabakhsh, and D. Woodard, in Proc. 5th High Energy

Heavy Ion Summer Study, LBL-12652, Conf-8105104, Berkeley, May, 1981, p.470.

12. E. Aslanides, P. Fassnacht, F. Hibou, E. Chiavassa,G. Dellacasa, M. Gallio, A. Musso, T. Bressani, and G. Puddu, Phys. Rev. Lett. 43, 1466 (1979).
13. Yu. D. Bayukov, V. I. Efremenko, V. B. Fedorov, V. B. Gavrilov, G. A. Leskin, V. S. Pavlov, D. A. Suchkov, B. B. Shvartsmann, and Yu. M. Zaitsev, ITEP preprint, ITEP-49 (1977).
14. P. B. Price and J. Stevenson, Phys. Rev. Lett. 34, 405 (1975).
15. R. L. Holt, J. P. Schiffer, J. Specht, L. M. Bollinger, and G. E. Thomas, Phys. Rev. Lett. 36, 183 (1976).
16. P. J. Siemens and J. I. Kapusta, Phys. Rev. Lett. 43, 1486 (1979); 43, 1690 (1979) (E).
17. I. N. Mishustin, F. Myhrer, and P. J. Siemens, Phys. Lett. 95B, 361 (1980).
18. L. P. Csernai and H. W. Barz, Z. fur Physik A296, 173 (1980).
19. J. I. Kapusta and D. Strottman, Phys. Rev. C23, 1282 (1981).
20. G. Bertsch and J. Cugnon, preprint (1981).
21. H. Stöcker, Lawrence Berkeley Laboratory Report LBL-12302 (1981).
22. E. M. Friedlander, R. W. Gimpel, H. H. Heckman, Y. Karant, B. Judek, and E. Ganssauge, Phys. Rev. Lett. 45, 1084 (1980).
23. M. Gyulassy, Nucl. Phys. A354, 395 (1981).
24. S. E. Koonin, Phys. Rev. Lett. 39, 680 (1977).
25. I. A. Schmidt and R. Blankenbecler, Phys. Rev. D15, 3321 (1977); Phys. Rev. D16, 1318 (1977).
26. G. Bertsch, Phys. Rev. C15, 713 (1977).
27. R. L. Hatch and S. E. Koonin, Phys. Lett. 81B, 1 (1978).
28. R. H. Landau and M. Gyulassy, Phys. Rev. C19, 149 (1979).
29. M. Chemtob, Nucl. Phys. A314, 387 (1979); Nucl. Phys. A336, 299 (1979).
30. B. K. Jain, Phys. Rev. C22, 583 (1980).
31. M. Sobel, P. J. Siemens, J. P. Bondorf, and H. A. Bethe, Nucl. Phys. A251, 502

(1975).

32. G. D. Westfall, J. Gosset, P. J. Johansen, A. M. Poskanzer, W. G. Meyer, H. H. Gutbrod, A. Sandoval, and R. Stock, Phys. Rev. Lett. 37, 1202 (1976).
33. J. Gosset, H. H. Gutbrod, W. G. Meyer, A. M. Poskanzer, A. Sandoval, R. Stock, and G. D. Westfall, Phys. Rev. C16, 629 (1977).
34. J. I. Kapusta, Phys. Rev. C16, 1493 (1977).
35. A. Z. Mekjian, Phys. Rev. Lett. 38, 640 (1977); Phys. Rev. C17, 1051 (1978); Nucl. Phys. A312, 491 (1978); Phys. Lett. 89B, 177 (1980).
36. W. D. Myers, Nucl. Phys. A296, 177 (1978).
37. J. Gosset, J. I. Kapusta, and G. D. Westfall, Phys. Rev. C18, 844 (1978).
38. S. Das Gupta, Phys. Rev. Lett. 41, 1450 (1978).
39. N. K. Glendenning and Y. Karant, Phys. Rev. Lett. 40, 374 (1978).
40. I. Montvay and J. Zimanyi, Nucl. Phys. A316, 490 (1979).
41. S. I. A. Garpman, N. K. Glendenning, and Y. J. Karant, Nucl. Phys. A322, 382 (1979).
42. I. G. Bofatskaya, C. B. Chiu, M. I. Gorenstein, and G. M. Zinovjev, Phys. Rev. C22, 209 (1980).
43. S. Das Gupta and A. Z. Mekjian, Phys. Reports 72, 131 (1981).
44. I. Tanihata, S. Nagamiya, S. Schnetzer, and H. Steiner, Phys. Lett. 100B, 121 (1981).
45. R. E. Chrien, T. J. Kriieger, R. J. Sutter, M. May, H. Palevsky, R. L. Stearns, T. Kozlowski, and T. Bauer, Phys. Rev. C21, 1014 (1980).
46. R. Hanbury-Brown and R. Q. Twiss, Nature 178, 1046 (1956).
47. G. Goldhaber, S. Goldhaber, W. Lee, and A Pais, Phys. Rev. 120, 300 (1960).
48. G. I. Kopylov, Phys. Lett. 50B, 572 (1974).
49. G. Cocconi, Phys. Lett. 49B, 459 (1974).
50. S. E. Koonin, Phys. Lett. 70B, 43 (1977).
51. F. B. Yano and S. E. Koonin, Phys. Lett. 78B, 556 (1978).
52. M. Gyulassy and S. K. Kauffmann, and L. W. Wilson, Phys. Rev. C20, 2267 (1979).

53. S. Y. Fung, W. Gorn, G. P. Kiernan, J. J. Lu, Y. T. Oh, and R. T. Poe, Phys. Rev. Lett. 41, 1592 (1978).

54. J. Bartke, Nucl. Phys. A335, 481 (1980).

55. J. J. Lu, D. Beavis, S. Y. Fung, W. Gorn, A. Huie, G. P. Kiernan, R. T. Poe, and G. VanDalen, Phys. Rev. Lett. 46, 898 (1981).

56. W. A. Zajc, J. A. Bistirlich, R. R. Bossingham, H. R. Bowman, C. W. Clawson, K. M. Crowe, K. A. Frankel, O. Hashimoto, J. G. Ingersoll, M. Koike, J. P. Kurck, C. J. Martoff, W. J. McDonald, J. P. Miller, D. Murphy, J. O. Rasmussen, J. P. Sullivin, P. Truol, and E. Yoo, in Proc. 5th High Energy Heavy Ion Summer Study, LBL-12652, Conf-8105104, Berkeley, May, 1981, p.350.

57. Z. Zarbakhsh, A. L. Sagle, F. Brochard, T. A. Mulera, V. Perez-Mendez, I. Tanihata, J. B. Carroll, K. S. Ganezer, G. Igo, J. Oostens, D. Woodard, and R. Sutter, Phys. Rev. Lett. 46, 1268 (1981).

58. S. Nagamiya, I. Tanihata, S. Schnetzer, L. Anderson, W. Brückner, O. Chamberlain, S. Schnetzer, G. Shapiro, and H. Steiner, J. Phys. Soc. Japan Suppl. 44, 378 (1978).

59. S. Nagamiya, L. Anderson, W. Brückner, O. Chamberlain, M.-C. Lemaire, S. Schnetzer, G. Shapiro, H. Steiner, and I. Tanihata, Phys. Lett. 81B, 147 (1979).

60. I. Tanihata, M.-C. Lemaire, S. Nagamiya, and S. Schnetzer, Phys. Lett. 97B, 363 (1980).

61. I. Tanihata, in Proceedings of Hakone Seminar on High-Energy Nuclear Interactions and Properties of Dense Nuclear Matter (K. Nakai and A. S. Goldhaber, ed.), p.382, Hakone, Japan, July, 1980.

62. J. Cugnon, Phys. Rev. C22, 1885 (1980).

63. J. Hüfner, in Proc. 4th High Energy Heavy Ion Summer Study, LBL-7766, Conf-780766, Berkeley, 1978, p.135.

64. P. Hecking and H. Pirner, Nucl. Phys. A333, 514 (1980).

65. J. Knoll, Phys. Rev. C20, 773 (1979).

66. S. Nagamiya, M.-C. Lemaire, S. Schnetzer, H. Steiner, and I. Tanihata, Phys. Rev. Lett. 45, 602 (1980).

67. A. Sandoval, R. Stock, H. E. Stelzer, R. E. Renfordt, J. W. Harris, J. P. Branniggan, J. V. Geaga, L. J. Rosenberg, L. S. Schroeder, and K. L. Wolf, Phys. Rev. Lett. 45, 874 (1980).

68. J. D. Bowman, W. J. Swiatecki, and C. F. Tsang, Lawrence Berkeley Laboratory Report LBL-2908 (1973), unpublished.

69. J. Hüfner and J. Knoll, Nucl. Phys. A290, 460 (1977).

70. S. Nagamiya, Nucl. Phys. A335, 517 (1980).

71. M. Gyulassy and S. K. Kauffmann, Phys. Rev. Lett. 40, 298 (1978).

72. R. Stock, H. H. Gutbrod, W. G. Meyer, A. M. Poskanzer, A. Sandoval, J. Gosset, C. H. King, G. King, Ch. Lucker, Nguyen Van Sen, G. D. Westfall, and K. L. Wolf, Phys. Rev. Lett. 44, 1243 (1980).

73. S. Y. Fung, W. Gorn, G. P. Kiernan, F. F. Liu, J. J. Lu, Y. T. Oh, J. Ozawa, R. T. Poe, L. S. Schroeder, and H. Steiner, Phys. Rev. Lett. 40, 292 (1978).

74. H. G. Baumgardt, J. U. Schott, Y. Sakamoto, E. Schopper, H. Stöcker, J. Hofmann, W. Scheid, and W. Greiner, Z. Physik A273, 359 (1975).

75. W. Scheid, H. Muller, and W. Greiner, Phys. Rev. Lett. 32, 741 (1974).

76. H. H. Heckman, H. J. Crawford, D. E. Greiner, P. J. Lindstrom, and Lance W. Wilson, Phys. Rev. C17, 1651 (1978).

77. H. Stöcker, J. A. Maruhn, and W. Greiner, Phys. Rev. Lett. 44, 725 (1980).

78. H. Stöcker, C. Riedel, Y. Yariv, L. P. Csernai, G. Buchwald, G. Graebner, J. A. Maruhn, W. Greiner, K. Frankel, M. Gyulassy, B. Schürmann, G. Westfall, J. D. Stevenson, J. R. Nix, and D. Strottman, Phys. Rev. Lett. 47, 1807 (1981).

79. J. R. Nix and D. Strottman, Phys. Rev. C23, 2548 (1981).

80. H. Stöcker *et al.*, Lawrence Berkeley Laboratory Report LBL-11774 (1980).

81. Y. Yariv and Z. Fraenkel, Phys. Rev. C20, 2227 (1979).

82. J. D. Stevenson, Phys. Rev. Lett. 41, 1702 (1978); Phys. Rev. Lett. 45, 1773 (1980).

83. M. Chemtob and B. Schürmann, Nucl. Phys. A336, 508 (1980).

84. B. Schürmann and M. Chemtob, Z. Physik A294, 371 (1980).

85. L. P. Csernai and W. Greiner, Phys. Lett. 99B, 85 (1981).

86. L. P. Csernai, W. Greiner, H. Stöcker, I. Tanihata, S. Nagamiya, and J. Knoll, Phys. Rev. C (in press) [Preprint Lawrence Berkeley Laboratory Report LBL-13944 (1981)].

87. J. Knoll, Phys. Rev. C20, 773 (1979).

88. P. J. Siemens and J. O. Rasmussen, Phys. Rev. Lett. 42, 844 (1979).

89. J. I. Kapusta and D. Strottman, Phys. Rev. C23, 1282 (1981).

90. B. Schürmann and N. Macoc-Borstnik, preprint (1981).

91. J. Randrup, Phys. Lett. 76B, 547 (1978).

92. S. Nagamiya *et al.*, Bevatron-Bevalac Experiment 512H.

93. S. Frankel, Phys. Rev. Lett. 38, 1338 (1977); Phys. Rev. C17, 697 (1978).

94. R. D. Amado and R. M. Woloshyn, Phys. Rev. Lett. 36, 1435 (1976); Phys. Lett. 69B, 400 (1977).

95. A. M. Baldin, AIP Conference Proceedings 26, 621 (1975) and references therein.

96. V. V. Burov, V. K. Lukyanov, and A. I. Titov, Phys. Lett. 67B, 46 (1977).

97. T. Fujita, Phys. Rev. Lett. 39, 174 (1977); Nucl. Phys. A324, 409 (1979).

98. T. Fujita and J. Hüfner, Nucl. Phys. A314, 317 (1979).

99. V. I. Komorov, G. E. Kosarev, H. Muller, D. Netzband, V. D. Toneev, T. Stiehler, S. Tesch, K. K. Gudima, and S. G. Mashnik, Nucl. Phys. A326, 297 (1979).

100. I. Tanihata, Y. Miake, H. Hamagaki, S. Kadota, Y. Shida, R. Lombard, E. Moeller, S. Nagamiya, S. Schnetzer, and H. Steiner, in Proceedings of the 5th High Energy Heavy Ion Summer Study, LBL-12652, Conf-8105104, Berkeley, May, 1981, p.365.

101. Preliminary data have been obtained from the group of Ref. 101.

102. A. R. Bodmer, Phys. Rev. D4, 1601 (1974).

103. T. D. Lee and G. C. Wick, Phys. Rev. D9, 2291 (1974).

104. T. D. Lee, Rev. Mod. Phys. 47, 267 (1976) and references therein.

105. W. Weise and G. E. Brown, Phys. Reports 27C, 1 (1976) and references therein.

106. A. B. Migdal, Rev. Mod. Phys. 50, 107 (1978) and references therein.

107. V. Ruck, M. Gyulassy, and W. Greiner, Z. Phys. A277, 391 (1979).

108. G. G. Bunatjan, Yad. Fiz. 29, 258 (1979) [Sov. J. Nucl. Phys. 30, 131 (1979)].

109. W. Scheid, H. Muller, and W. Greiner, Phys. Rev. Lett. 32, 741 (1974).

110. C. F. Chapline, H. H. Johnson, E. Teller, and M. S. Weiss, Phys. Rev. D8, 4302 (1973).

111. H. Stöcker, J. Maruhn, and W. Greiner, Z. Physik A286, 121 (1978); Phys. Lett. 81B, 303 (1979).

112. K. K. Gudima and V. D. Toneev, Dubna Report E2-12644 (1979).

113. L. A. Kondratyuk and I. S. Shapiro, Yad. Fiz. 12, 401 (1970) [Soviet J. Nucl. Phys. 12, 220 (1971)].

114. J. Boguta, Lawrence Berkeley Laboratory Report LBL-12333 (1981), to be published.

115. N. K. Glendenning, Lawrence Berkeley Laboratory Report LBL-13611 (1981), to be published.

116. S. Nagamiya *et al.*, Bevatron-Bevalac Experiment 634H.

117. H. Spinka, in Proceedings of the Workshop on Nuclear and Particle Physics up to 31 GeV, Los Alamos Scientific Laboratory Report LA-8775-C, Los Alamos, January, 1981, p. 220.

118. F. J. Dyson and N.-H. Xuong, Phys. Rev. Lett. 13, 815 (1964).

119. T. Kamae and T. Fujita, Phys. Rev. Lett. 38, 471 (1977).

120. M. Oka and K. Yazaki, Phys. Lett. 90B, 41 (1980).

121. M. Cvetic, B. Golli, N. Mankoc-Borstnik, and M. Rosina, Phys. Lett. 93B, 489 (1980).

122. M. Rosina and H. J. Pirner, Nucl. Phys. A367, 398 (1981).

123. S. A. Chin and A. K. Kerman, Phys. Rev. Lett. 43, 1292 (1979).

124. T. J. M. Symons, V. P. Viyogi, G. D. Westfall, P. Doll, D. E. Greiner, H. Faraggi, P. J. Lindstrom, D. K. Scott, H. J. Crawford, and C. McParland, Phys. Rev. Lett. 42, 40 (1979).

125. G. D. Westfall, T. J. M. Symons, D. E. Greiner, H. H. Heckman, P. J. Lindstrom, J. Mahoney, A. C. Shotter, D. K. Scott, H. J. Crawford, C. McParland, T. C. Awes, C. K. Gelbke, and J. M. Kidd, Phys. Rev. Lett. 43, 1859 (1979).

126. M. R. Maier, H. G. Ritter, and H. H. Gutbrod, IEEE Tanns. on Nuclear Science NS-27, 42 (1980).

127. J. Gosset, in Proc. 1981 INS International Symposium on Nuclear Radiation Detectors (K. Husimi and Y. Shida, ed.), p.643, Tokyo, Japan, 1981.

128. K. Van Bibber and A. Sandoval, to be published in Heavy Ion Science, Plenum Press, New York, 1982.

129. B. Brandt and H. Dahman, Z. Phys. C1, 61 (1979).

130. H. Pirner, Phys. Rev. C22, 1962 (1980).

131. J. Kapusta and D. Strottman, Phys. Lett. (in press).

132. S. L. Wu and G. Zoberning, Z. Phys. C2, 107 (1979).

133. C. Y. Wong, Phys. Lett. 88B, 39 (1979).

134. HISS Conceptional Design Report, Lawrence Berkeley Laboratory Report LBL-5004 (1978).

135. Y. Alexander, J. W. vanOrden, E. F. Resish, and S. J. Wallace, Phys. Rev. Lett. 44, 1579 (1980).

136. J. Knoll and J. Randrup, Phys. Lett. 103B, 264 (1981).

Figure Captions

FIG. 1 A streamer chamber photograph taken by the U.C. Riverside group in 1.8 A·GeV Ar + Pb collisions.

FIG. 2 The experimental layout for large-angle two-proton correlation experiment. Symbols U, D and R used in the text are *UP*, *DOWN*, and *RIGHT* telescopes, respectively, in this figure. They are plastic scintillator telescopes with absorbers sandwiched in between. The symbol S used in the text is the magnetic spectrometer which consists of a C magnet, multiwire proportional chambers (P1-P5), and plastic scintillators (G1-G3). For details of the spectrometer, see Ref. 6.

FIG. 3 (a) Inclusive proton spectra from p + C collisions at E_{Beam} = 800 MeV. Arrows indicate the momenta expected from pp or pn quasi-elastic scatterings.

(b) The 40° spectra from the same reaction. Inclusive, in-plane coincidence ($R \cdot S$), and out-of-plane coincidence ($U \cdot S$ or $D \cdot S$) spectra are plotted. Curve A shows the results of PWIA calculations (Ref. 135) and curves B, C, and D are the results of the linear cascade calculations (Ref. 136).

Figure taken from Ref. 44.

FIG. 4 Target-mass dependence of inclusive single-proton quasi-elastic-scattering cross sections (upper) and that of two-proton quasi-elastic scattering cross sections (lower). Black points are from Ref. 44 and open circles are from Ref. 45. Figure taken from Ref. 44.

FIG. 5 Recent results of two-pion interferometry in 1.8 A·GeV Ar + KCl collisions by Zajc *et al.* (Ref. 56). The normalization of the data was adjusted to fit Eq. (6) for the upper two graphs, but taken as free parameters for the lower two graphs. Raw data (upper left) show a broader width than the Coulomb corrected data (upper right). Lower two graphs are Coulomb corrected data for both $\pi^-\pi^-$ and $\pi^+\pi^+$.

Figure taken from Ref. 56.

FIG. 6 Recent results of two-proton correlations in 1.8 A·GeV Ar + KCl collisions by Zarbakhsh *et al.* (Ref. 57). Figure taken from Ref. 57.

FIG. 7 Large-angle two-proton correlation data in 800 A·MeV C + C collisions. Values of the ratio C defined by Eq. (7) are plotted as a function of the proton momentum measured by the spectrometer, S. The solid line is the calculated result from the hard scattering model. The absolute value of this curve is 1/6 times the calculated one. Data are taken from Ref. 60.

FIG. 8 Multiplicity correlation between negative pions and charged nuclear fragments in 1.8 A·GeV Ar + KCl collisions (left), and that between negative pions and total charged particles in 1.8 A·GeV Ar + Pb collisions (right). Here, the total charged particles include nuclear fragments as well as positive and negative pions. Data are taken from Refs. 67 and 55.

FIG. 9 Average multiplicities $<m_\pi>$ for negative pions [Fig. 9 (a)] and average multiplicities $<m_Z>$ for nuclear charges [Fig. 9 (b)] determined from inclusive spectra. Here, P is the average nucleon number involved in the participant region, and P_Z is the average proton number involved in this region. Beam energies are 800 A·MeV. Data points were evaluated from the observed cross sections reported in Ref. 6.

FIG. 10 Pion multiplicity distribution at a fixed impact parameter. Events with $m_Z \geq$ 30 were selected in 1.8 A·GeV Ar + KCl collisions. Data were taken by Sandoval *et al.* (private communication).

FIG. 11 Angular distributions of low-energy protons for both low- and high-multiplicity events in 393 A·MeV Ne + U collisions. Figure taken from Ref. 72.

FIG. 12 The hydrodynamical side splash expected at a small impact parameter [Fig. 12 (a)], and the hydrodynamical bounce off expected at a large impact parameter [Fig. 12 (b)]. Figure taken from Ref. 77.

FIG. 13 Contour plot of the ratio C defined by Eq. (7) for two-proton emission in 800 A·MeV Ar + Pb collisions. Data are plotted in the (ϑ,E) plane, where ϑ and E are, respectively, the laboratory angle and energy of a proton detected by the spectrometer, S. For the experimental configuration, see also Fig. 14. Data are taken from Refs. 86 and 61.

FIG. 14 Experimental layout for the two-proton measurements in 800 A·MeV Ar + Pb collisions (upper figure), and the intuitive explanation for the data shown in Fig. 13 (lower figure).

FIG. 15 Proton and pion energy spectra for high-multiplicity events in 800 A·MeV Ar + KCl collisions. Fits to the data are based on the radial explosion model (Ref. 88). Figure taken from Ref. 66.

FIG. 16 Projectile and target mass dependence of proton emission in $A + A$ collisions. Invariant cross sections were parameterized to $\sigma \propto A^{\alpha}$, and values of α are plotted a function of the kinetic energy of protons. Data are taken from Ref. 6.

FIG. 17 Two possible mechanisms of the creation of high-p_T particles in nucleus-nucleus collisions.

FIG. 18 Two possible mechamisms of the creation of backward protons in proton-nucleus collisions.

FIG. 19 Schematical illustration of different mechanisms of backward proton emission that show up in the pp and pd momentum-momentum scatter plots.

FIG. 20 Experimental layout for the backward-forward coincidence experiments (Ref. 100) in proton-nucleus collisions.

FIG. 21 Momentum-momentum scatter plots between S (horizontal axis) and BI (vertical axis). Areas of black circles are porportional to the coincidence counts. Proton-proton (left) and proton-deuteron (right) coincidences are displayed.

FIG. 22 Backward proton spectra under various coincidence conditions.

FIG. 23 Hopes and goals of the research of high-energy nuclear collisions. Dynamical

path A indicates that most of the available energy is used to massive compression of nuclear matter whereas the path B indicates that it is used mainly to exciting nucleons into baryonic excited states.

FIG. 24 Time evolution of nuclear collisions calculated by cascade codes of Gudima and Toneev (Ref. 112), in the plane of τ (temperature) and n (density). The time scale of t is in units of 10^{-23} sec. Critical temperature $\tau(n)$ for pion condensation is also indicated by RGG (Ref. 107) and B (Ref. 108).

FIG. 25 A possibility of creating a Δ-soup in a Xe + Xe collision.

FIG. 26 The idea of a storage ring for production of neutron-rich-isotope beams. A thin target is prepared at the focusing point along the ring. Most of the time particles that hits the target experience no interactions. Then, these particles are again re-accelerated through the section of the "Slight acceleration" to compensate the energy loss through the target. Once some isotopes are created at the target, and in addition, if the N/Z ratio of these isotopes is larger than the N/Z ratio of the beam, then such isotopes will automatically escape out of the ring, because the magnetic rigidity of such an isotope is larger than the beam rigidity.

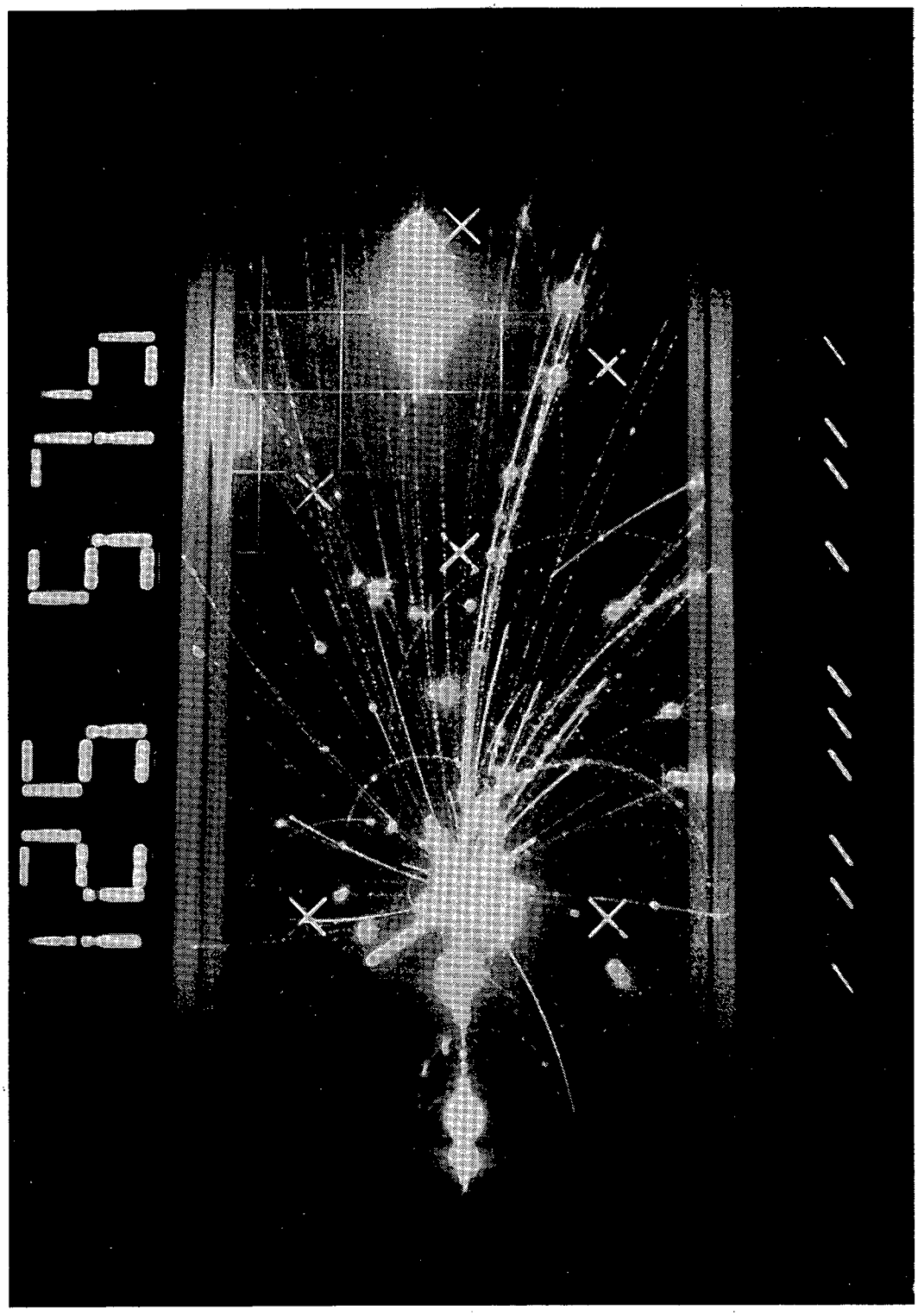

CBB 779-8983

Fig. 1

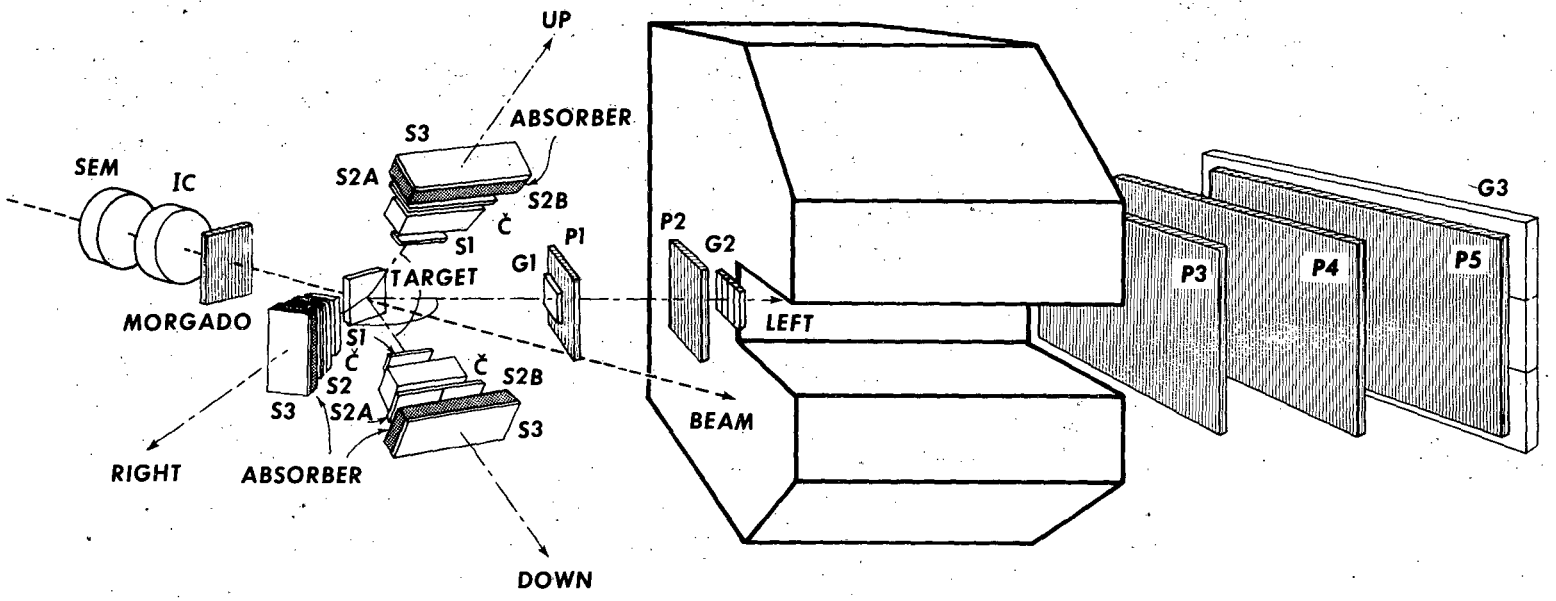

XBL769-4039

Fig. 2

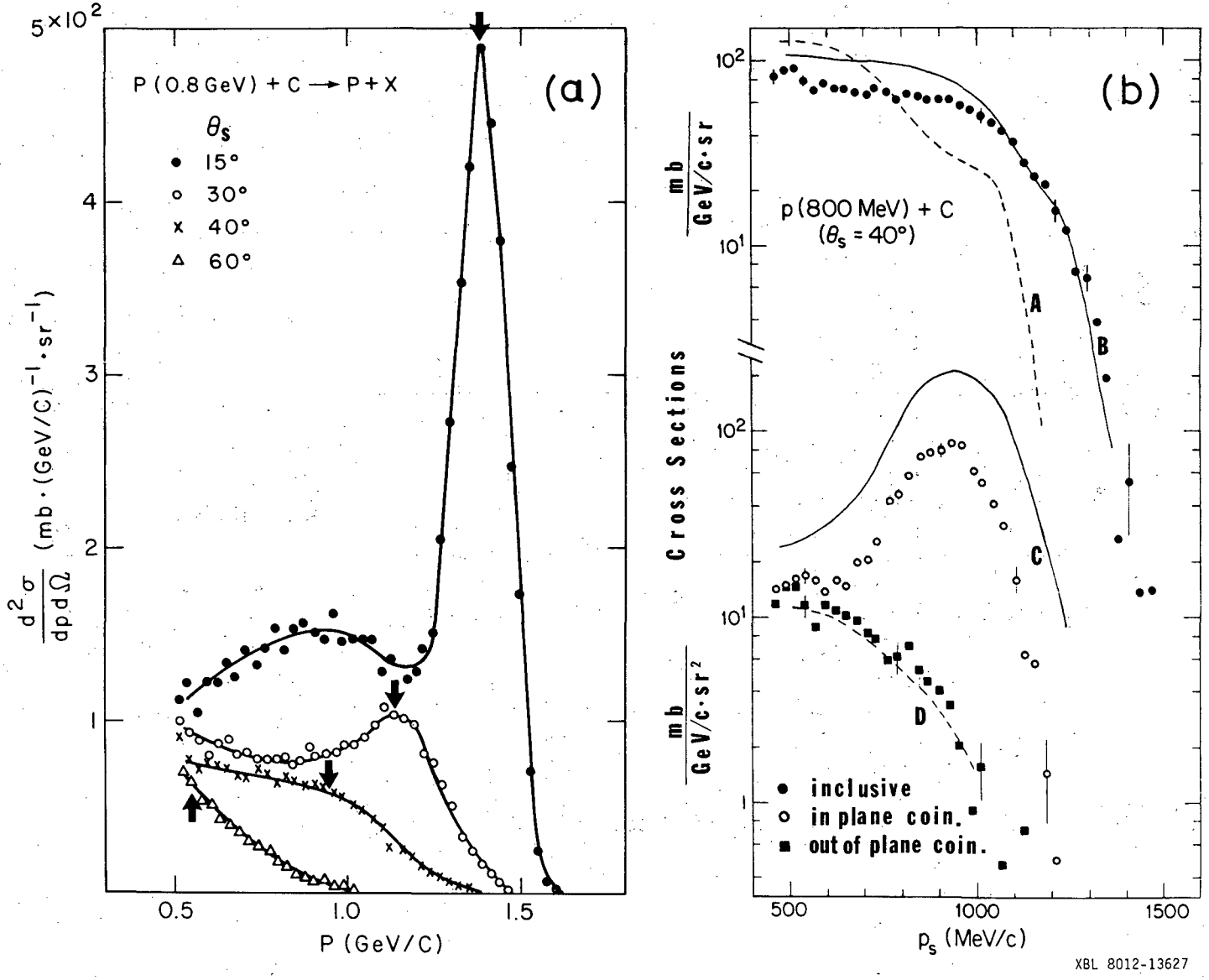
(a)
P (0.8 GeV) + C → P + X
θs
15°
30°
40°
60°
5×10²
4
3
2
1
0.5
1.0
1.5
P (GeV/C)
d²σ/dp dΩ (mb·(GeV/C)⁻¹·sr⁻¹)
(b)
p (800 MeV) + C
(θs = 40°)
A
B
C
D
inclusive
in plane coin.
out of plane coin.
mb/GeV/c·sr
mb/GeV/c·sr²
Cross Sections
10²
10¹
1
500
1000
1500
ps (MeV/c)
XBL 8012-13627

Fig. 3

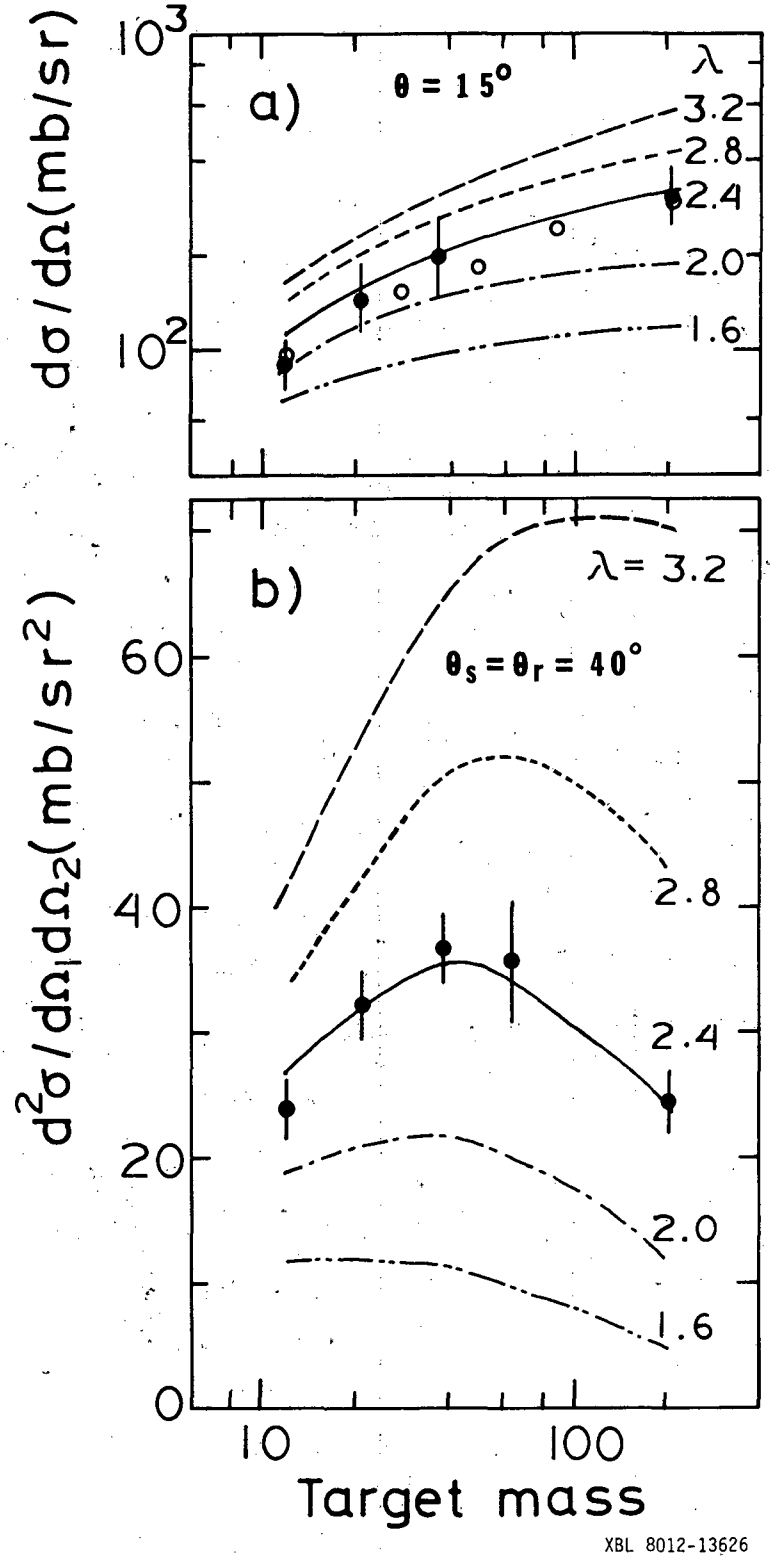
a)
θ = 15°
λ
3.2
2.8
2.4
2.0
1.6
10³
10²
dσ/dΩ(mb/sr)
b)
λ= 3.2
θs = θr = 40°
2.8
2.4
2.0
1.6
60
40
20
0
d²σ/dΩ1dΩ2(mb/sr²)
10
100
Target mass
XBL 8012-13626

Fig. 4

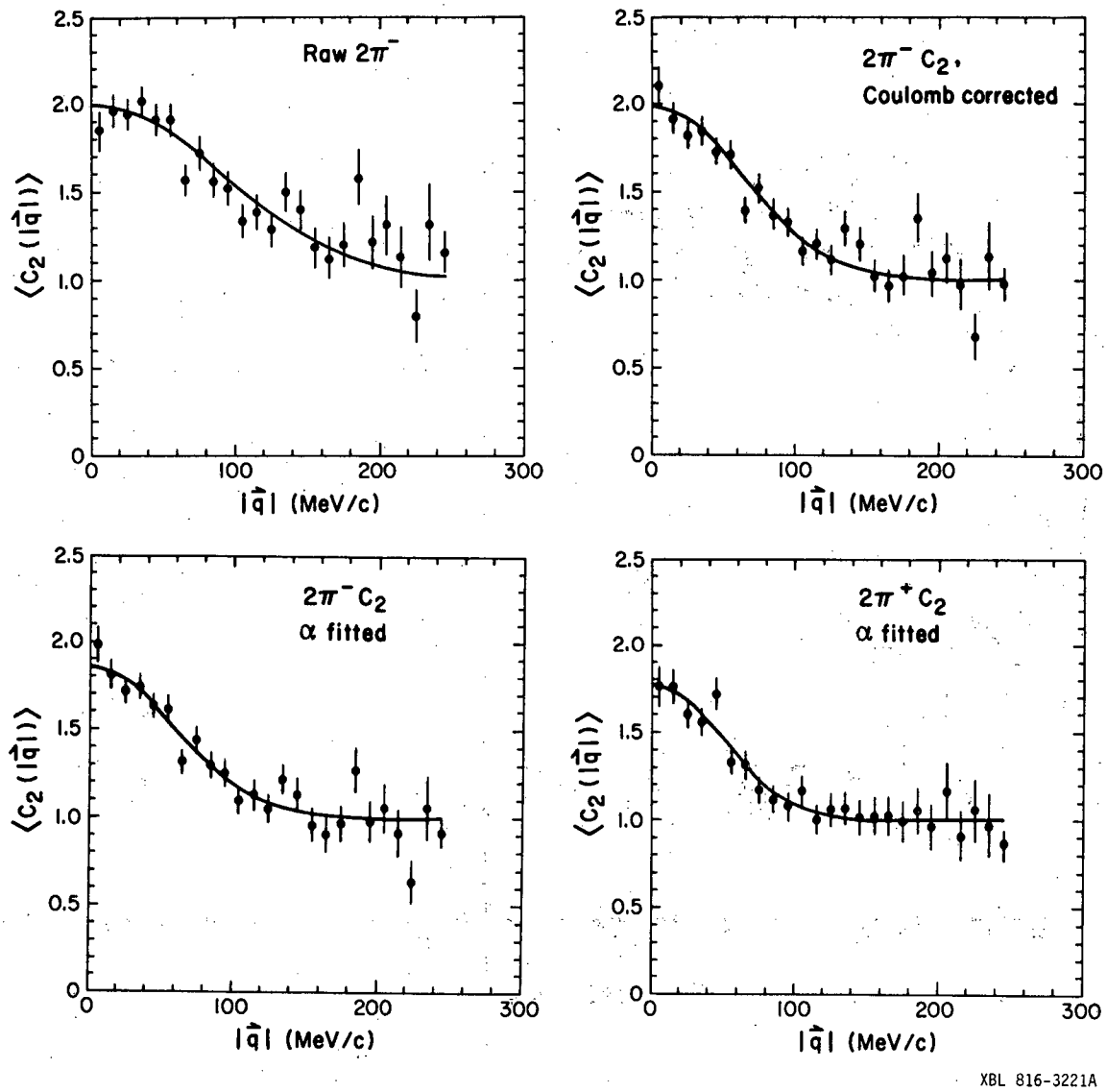
Raw $2\pi^-$
$2\pi^-$ C_2, Coulomb corrected
$2\pi^-$ C_2 α fitted
$2\pi^+$ C_2 α fitted
$\langle C_2(|\vec{q}|)\rangle$
$|\vec{q}|$ (MeV/c)
0
0.5
1.0
1.5
2.0
2.5
100
200
300
XBL 816-3221A

Fig. 5

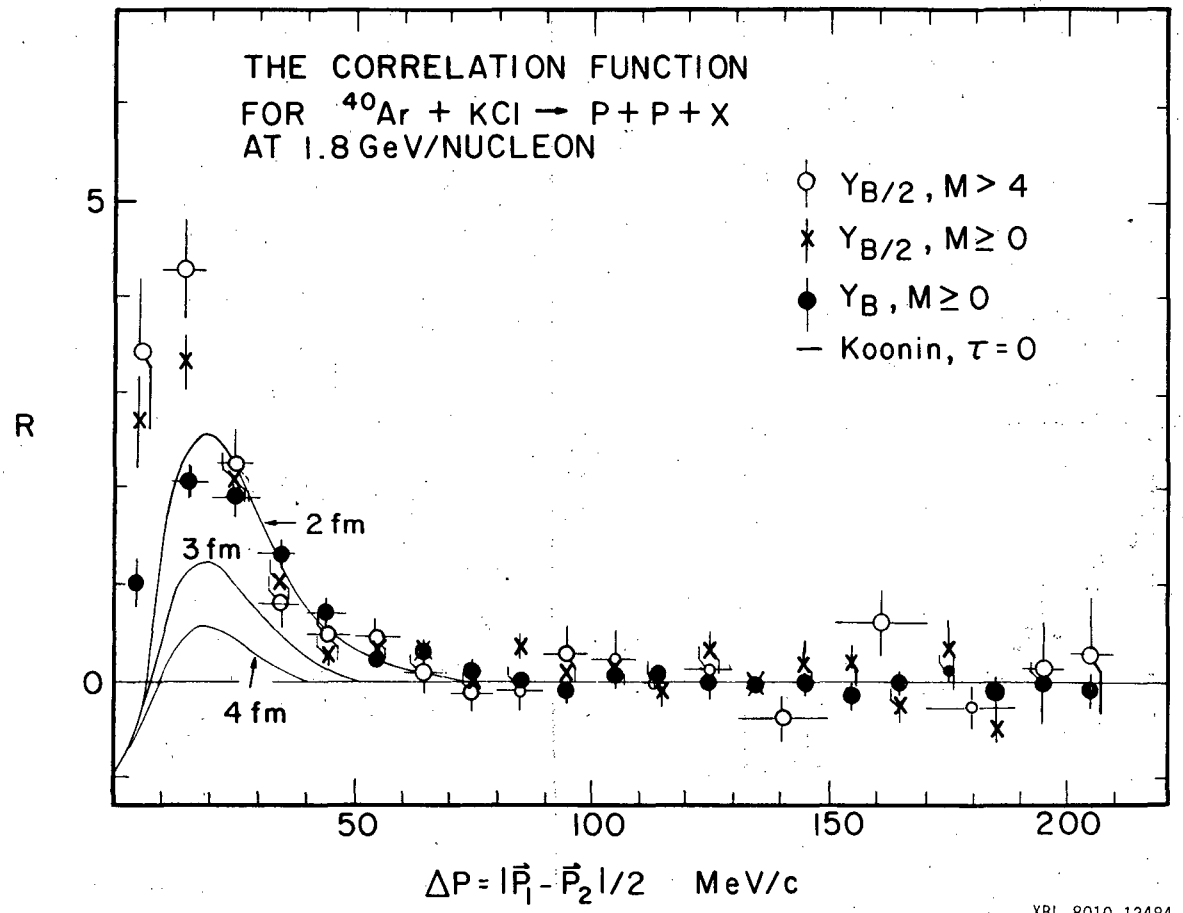

FIGURE 2

Fig. 6.

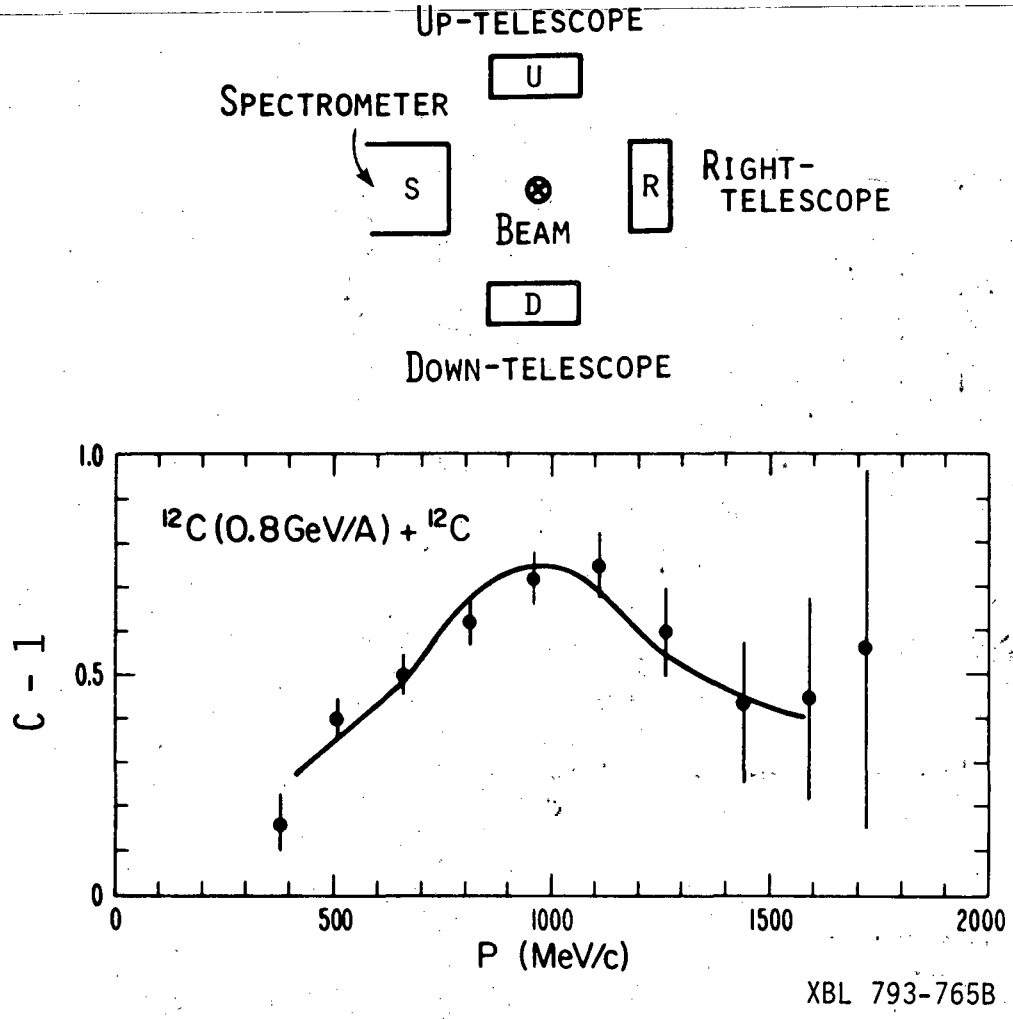
UP-TELESCOPE
U
SPECTROMETER
S
BEAM
R
RIGHT-
TELESCOPE
D
DOWN-TELESCOPE
^{12}C (0.8GeV/A) + ^{12}C
C - 1
1.0
0.5
0
0
500
1000
1500
2000
P (MeV/c)
XBL 793-765B

Fig. 7

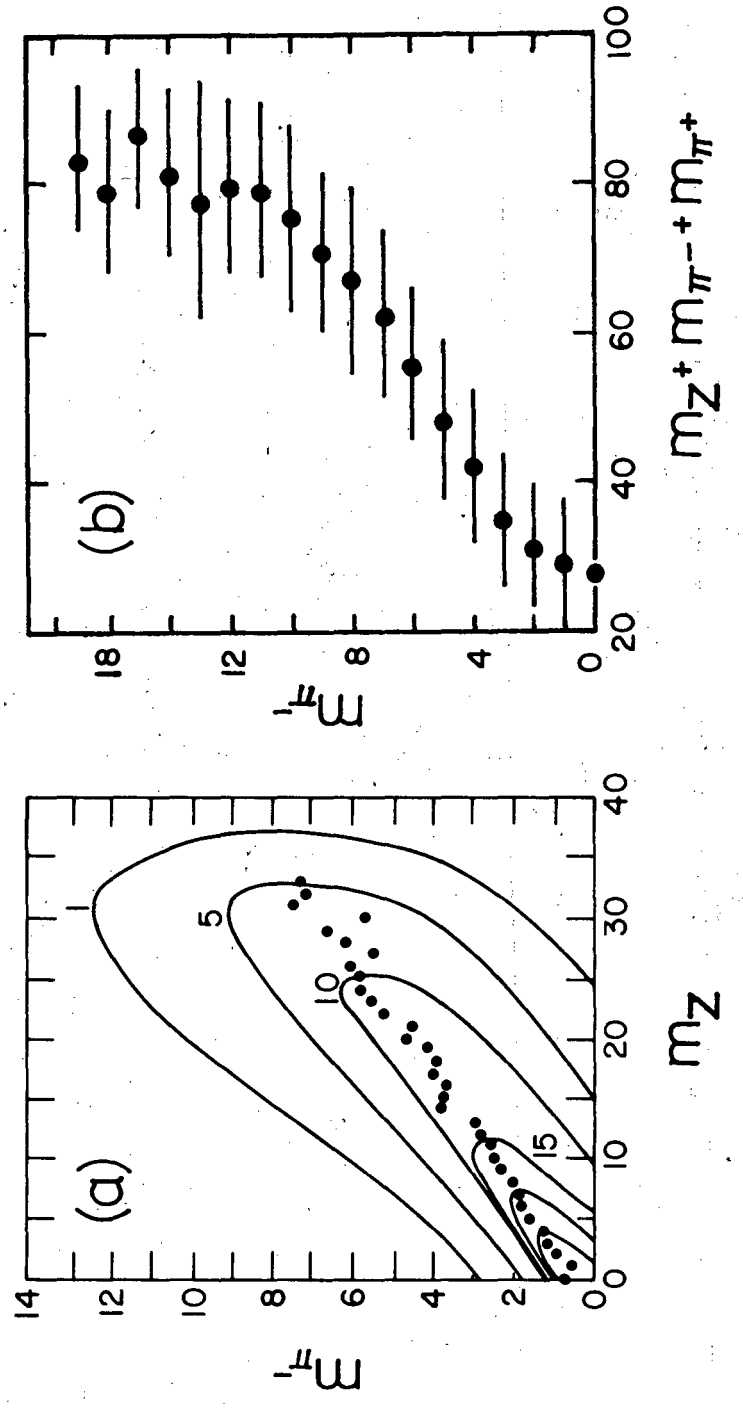

XBL 817-10509

Fig. 8

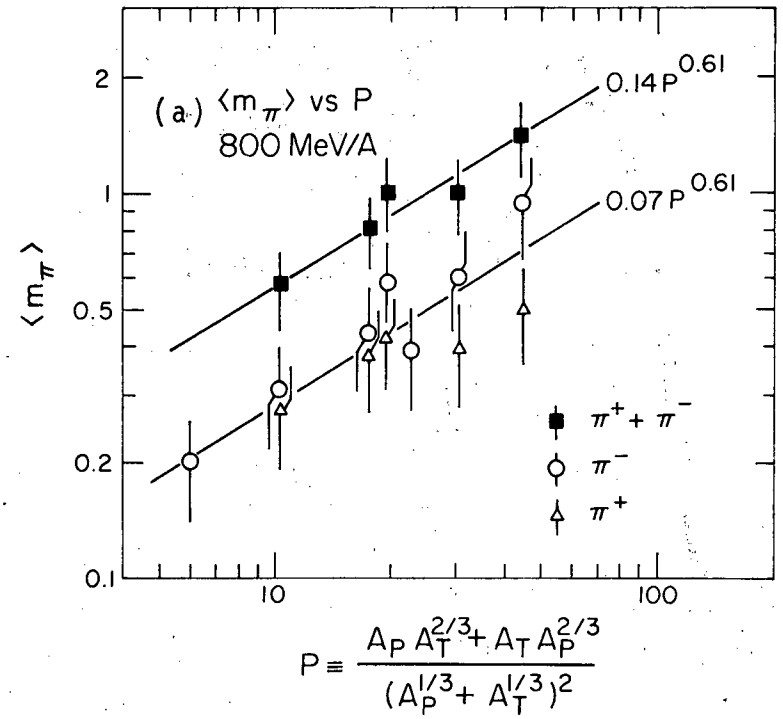

$$P \equiv \frac{A_P A_T^{2/3} + A_T A_P^{2/3}}{(A_P^{1/3} + A_T^{1/3})^2}$$

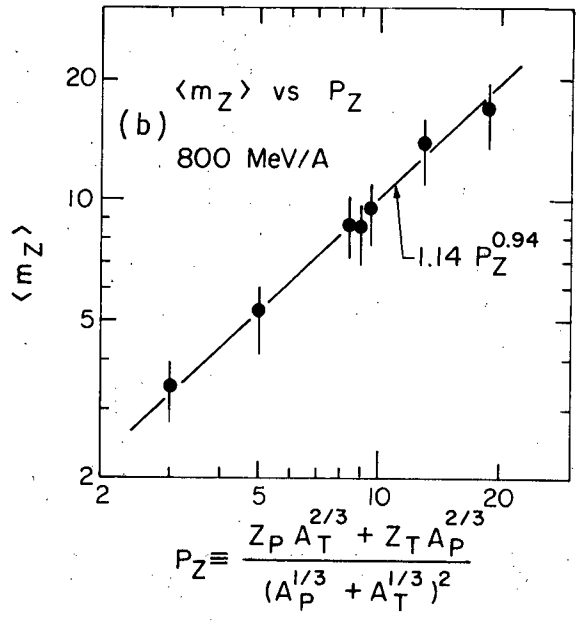

$$P_Z \equiv \frac{Z_P A_T^{2/3} + Z_T A_P^{2/3}}{(A_P^{1/3} + A_T^{1/3})^2}$$

XBL 816-2354A

Fig. 9

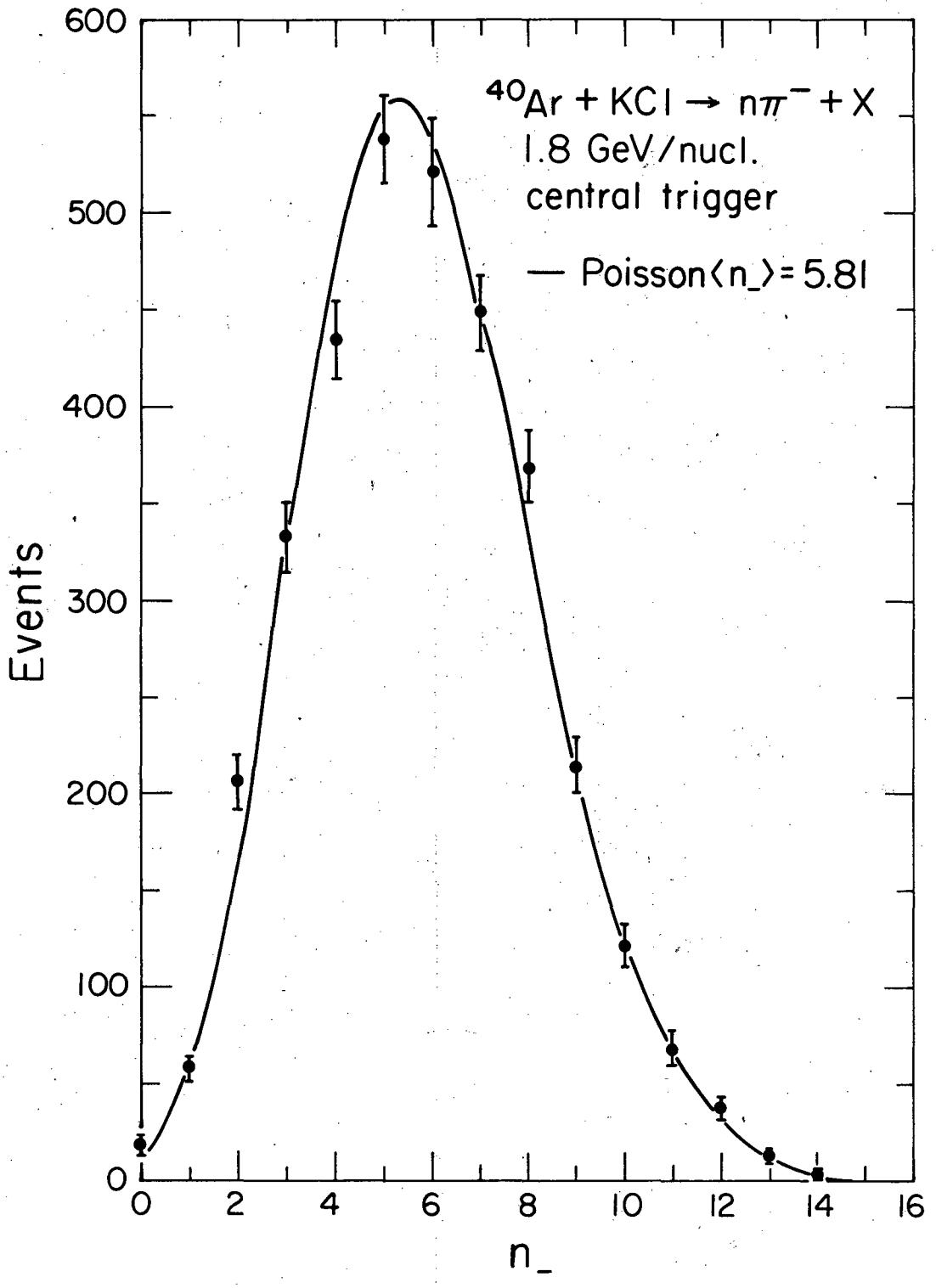

XBL 822-4454

Fig. 10

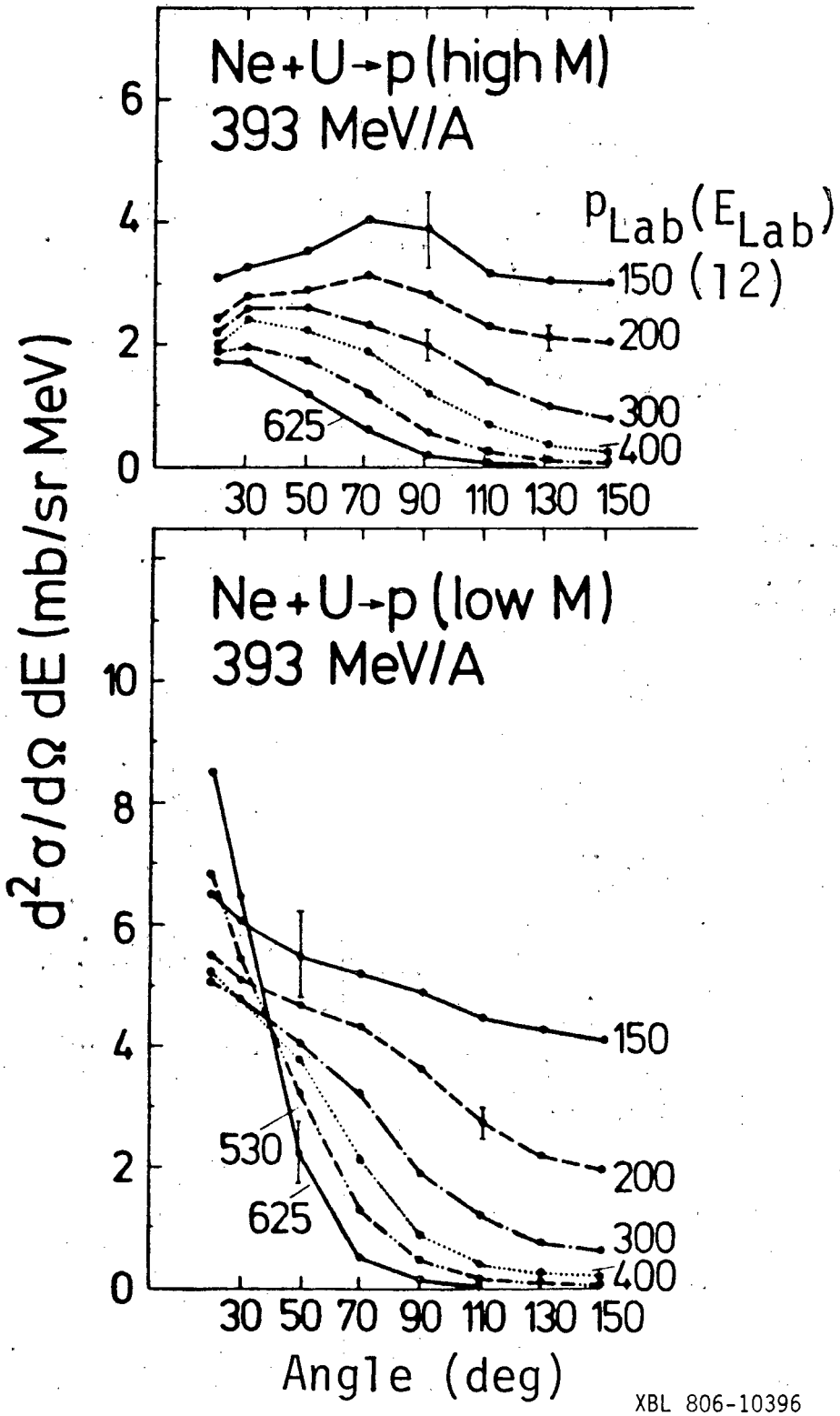
Ne+U→p (high M)
393 MeV/A
$p_{Lab}(E_{Lab})$
150 (12)
200
300
400
625
Ne+U→p (low M)
393 MeV/A
150
200
300
400
530
625
$d^2\sigma/d\Omega\, dE$ (mb/sr MeV)
Angle (deg)
XBL 806-10396

Fig. 11

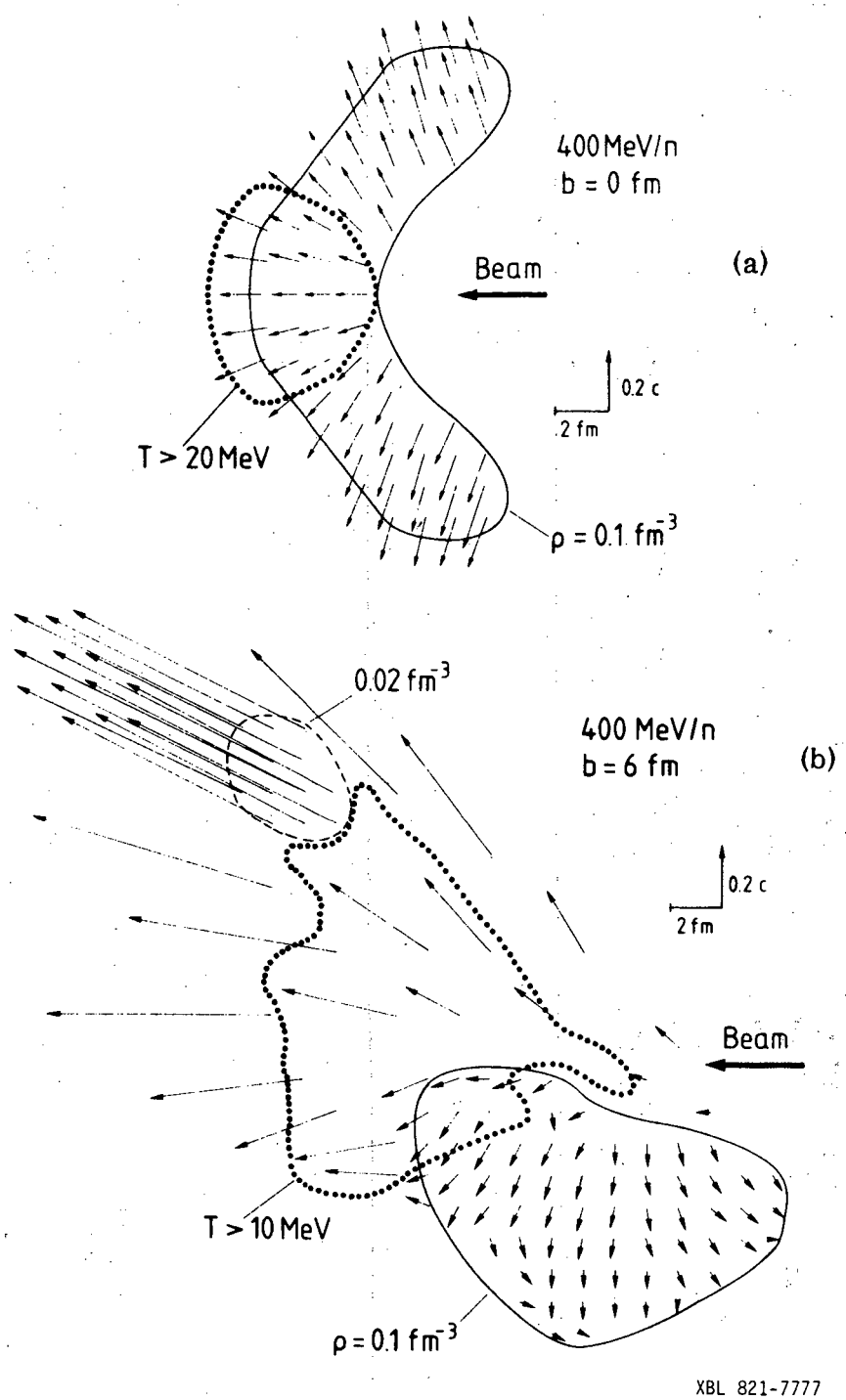
400 MeV/n
b = 0 fm
Beam
(a)
0.2 c
2 fm
T > 20 MeV
ρ = 0.1 fm⁻³
0.02 fm⁻³
400 MeV/n
b = 6 fm
(b)
0.2 c
2 fm
Beam
T > 10 MeV
ρ = 0.1 fm⁻³
XBL 821-7777

Fig. 12

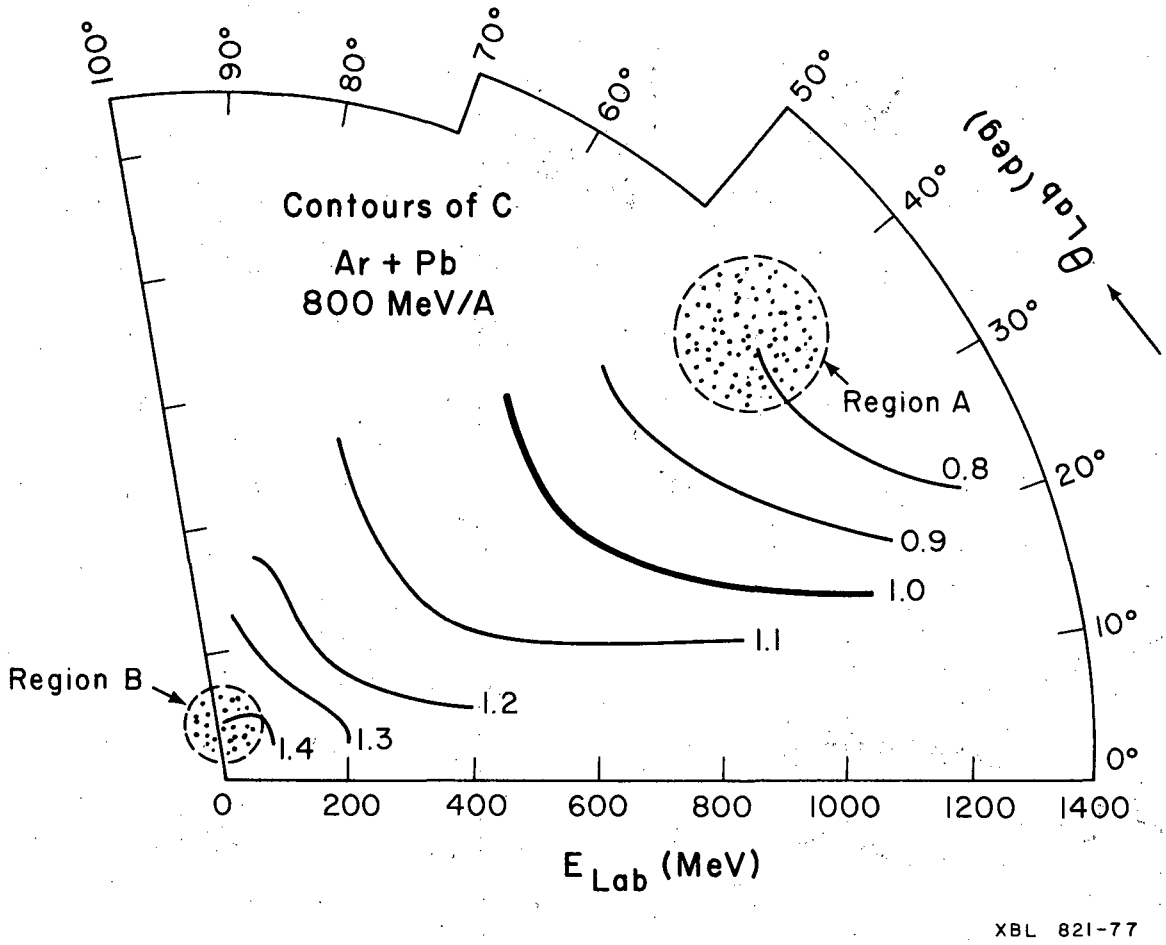

XBL 821-77

Fig. 13

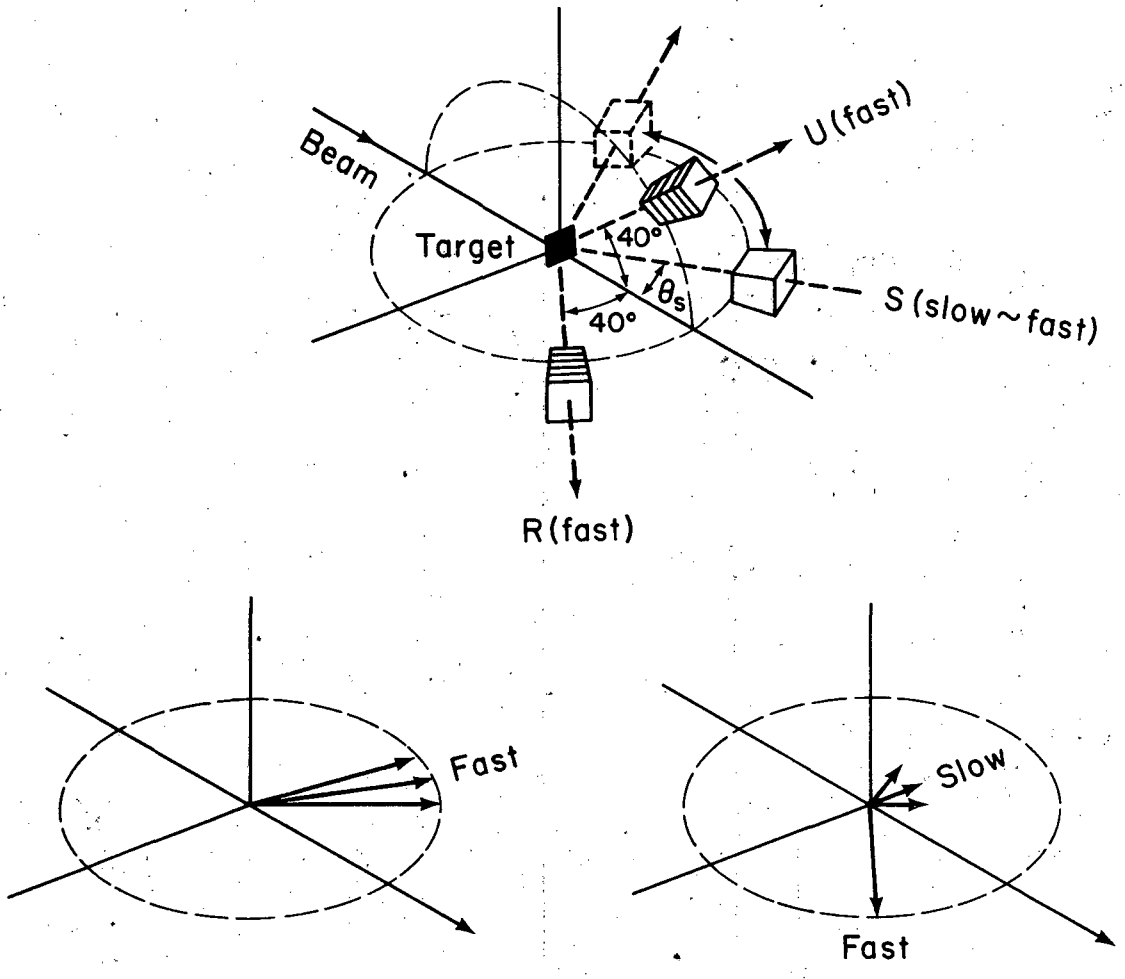

XBL 8112-13234

Fig. 14

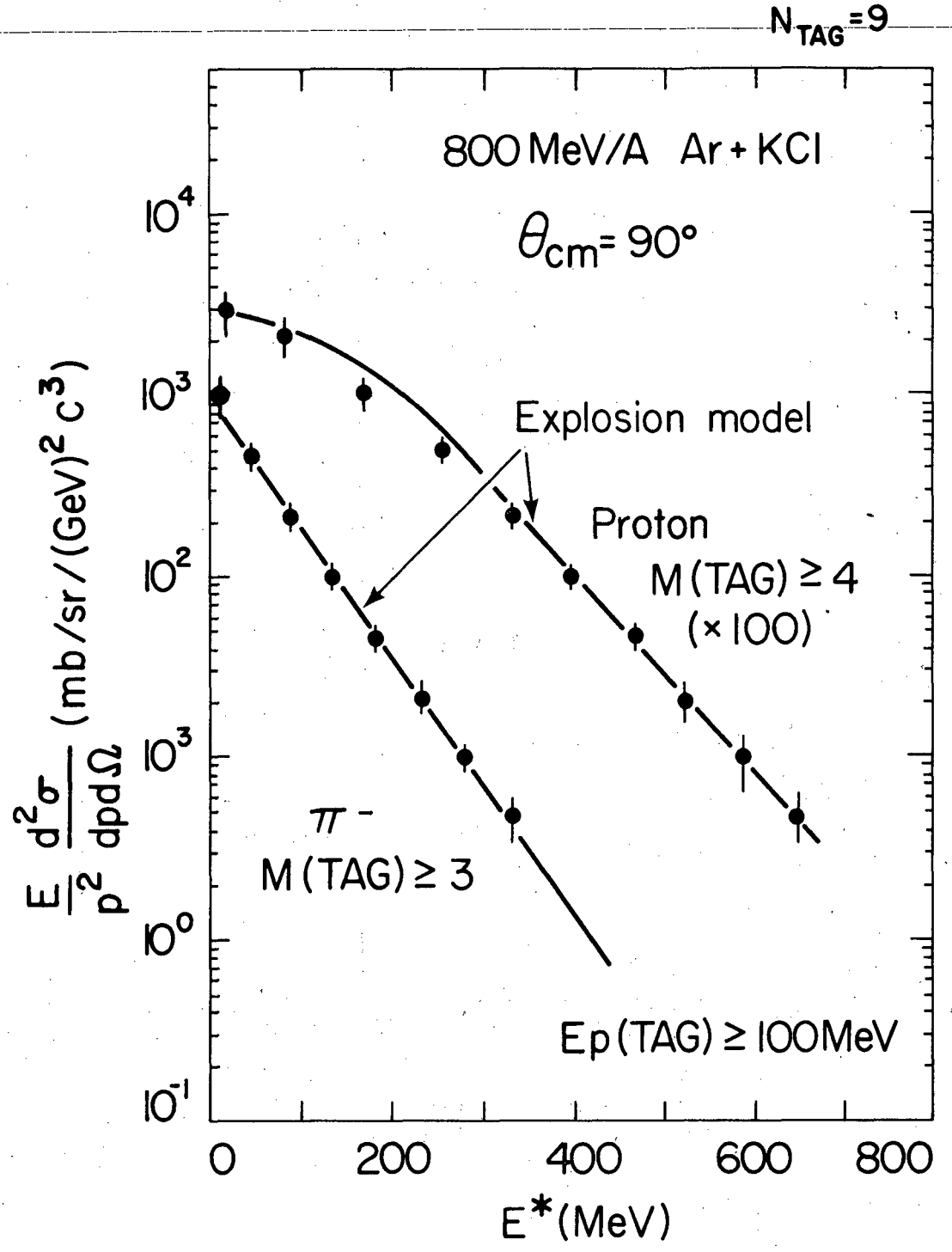

XBL 797 - 2130

Fig. 15

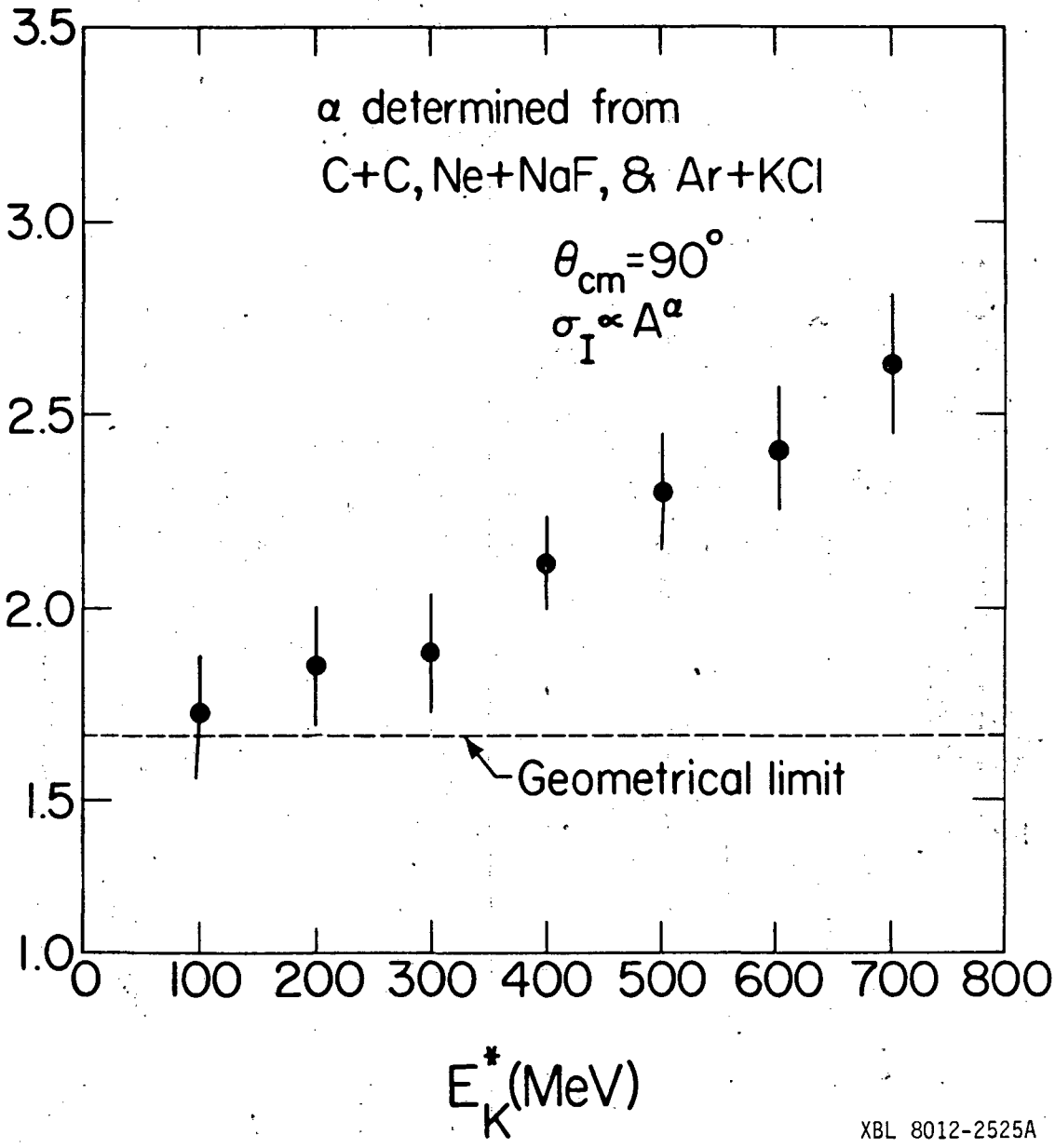
α determined from
C+C, Ne+NaF, & Ar+KCl
θ_{cm}=90°
$\sigma_I \propto A^{\alpha}$
Geometrical limit
3.5
3.0
2.5
2.0
1.5
1.0
0
100
200
300
400
500
600
700
800
E_K^*(MeV)
XBL 8012-2525A

Fig. 16

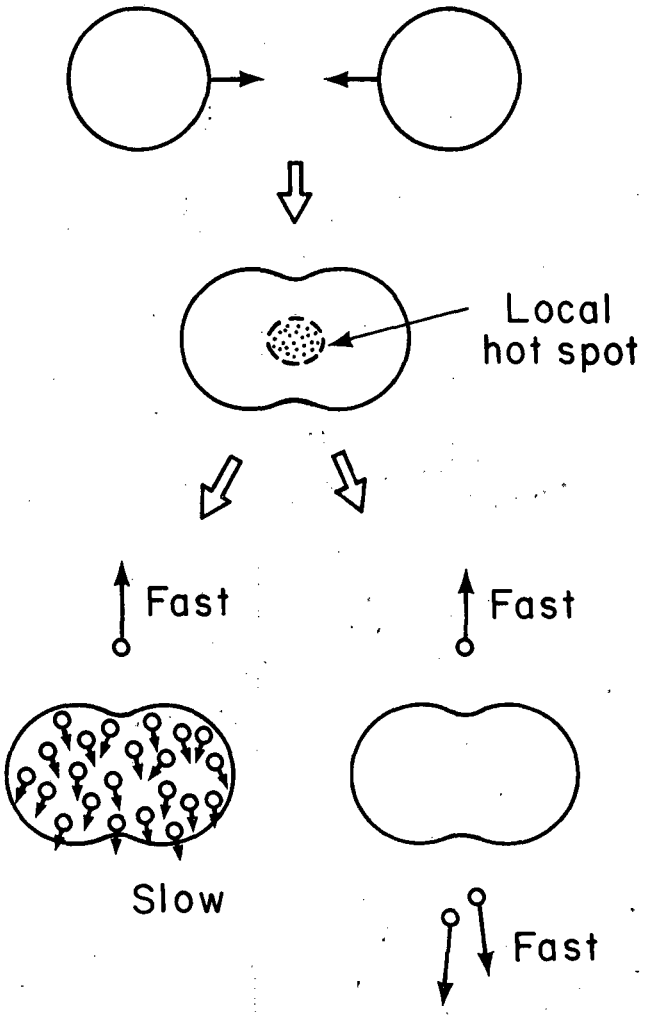

XBL 821-78

Fig. 17

Mechanism of backward proton emission in p + A collisions

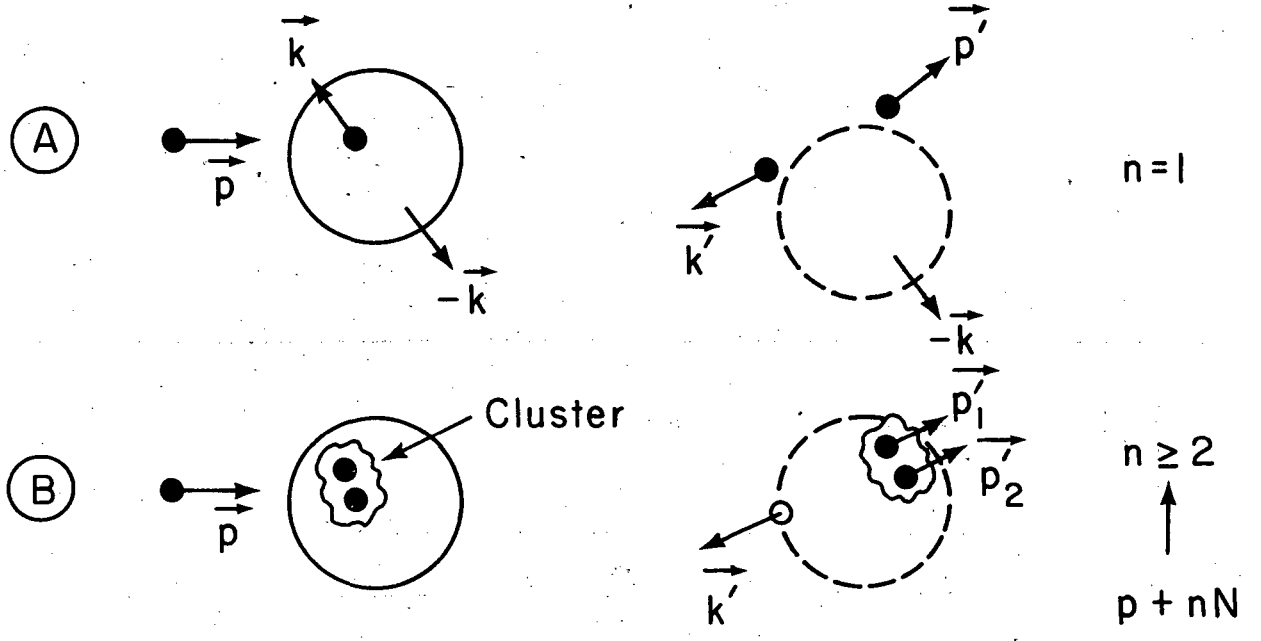

XBL 821-76

Fig. 18

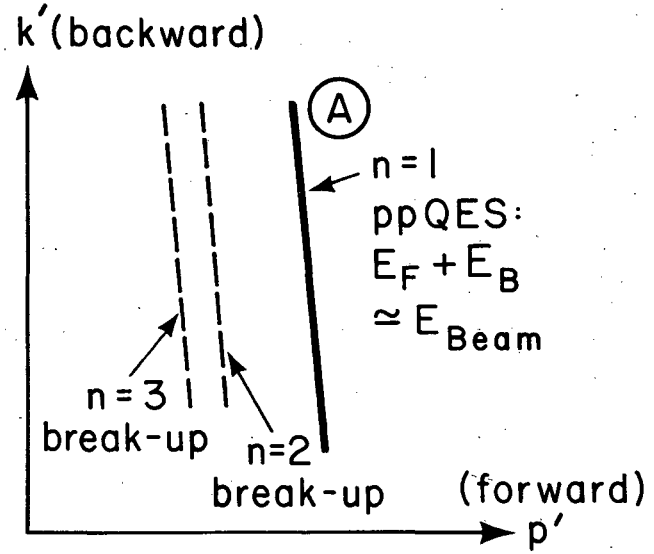

p-p Coincidences

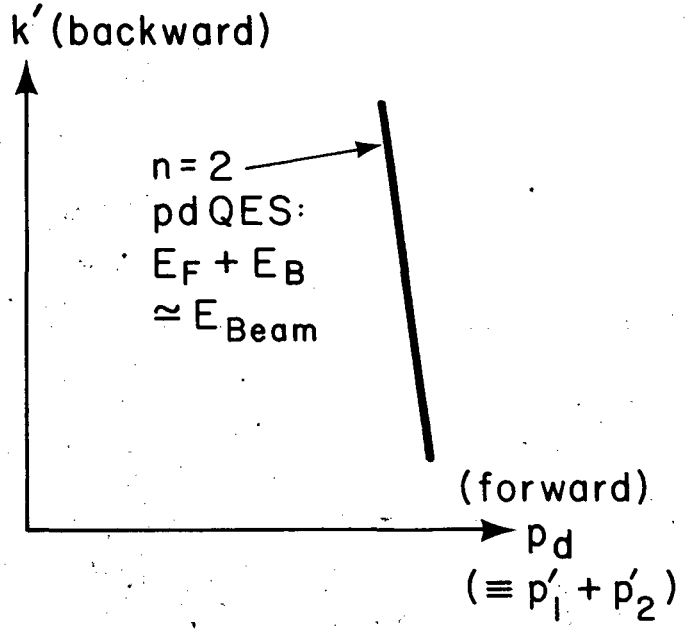

p-d Coincidences

XBL 821-79

Fig. 19

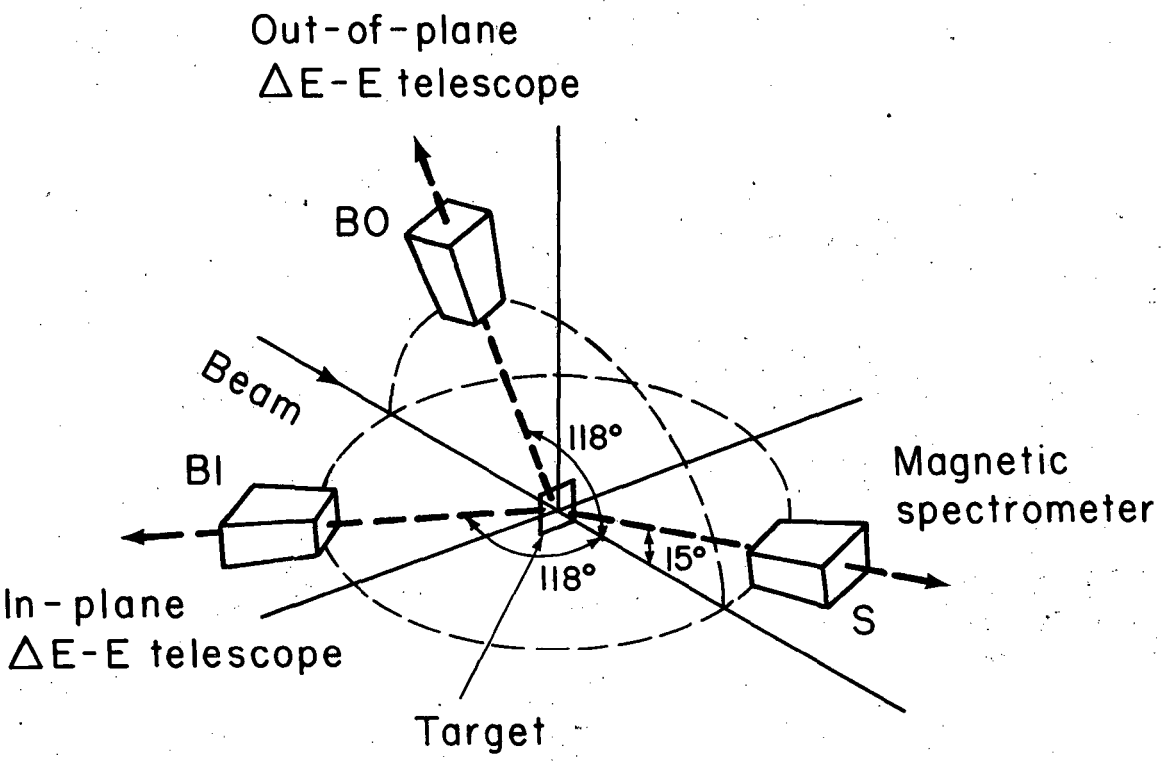

XBL 821-75

Fig. 20

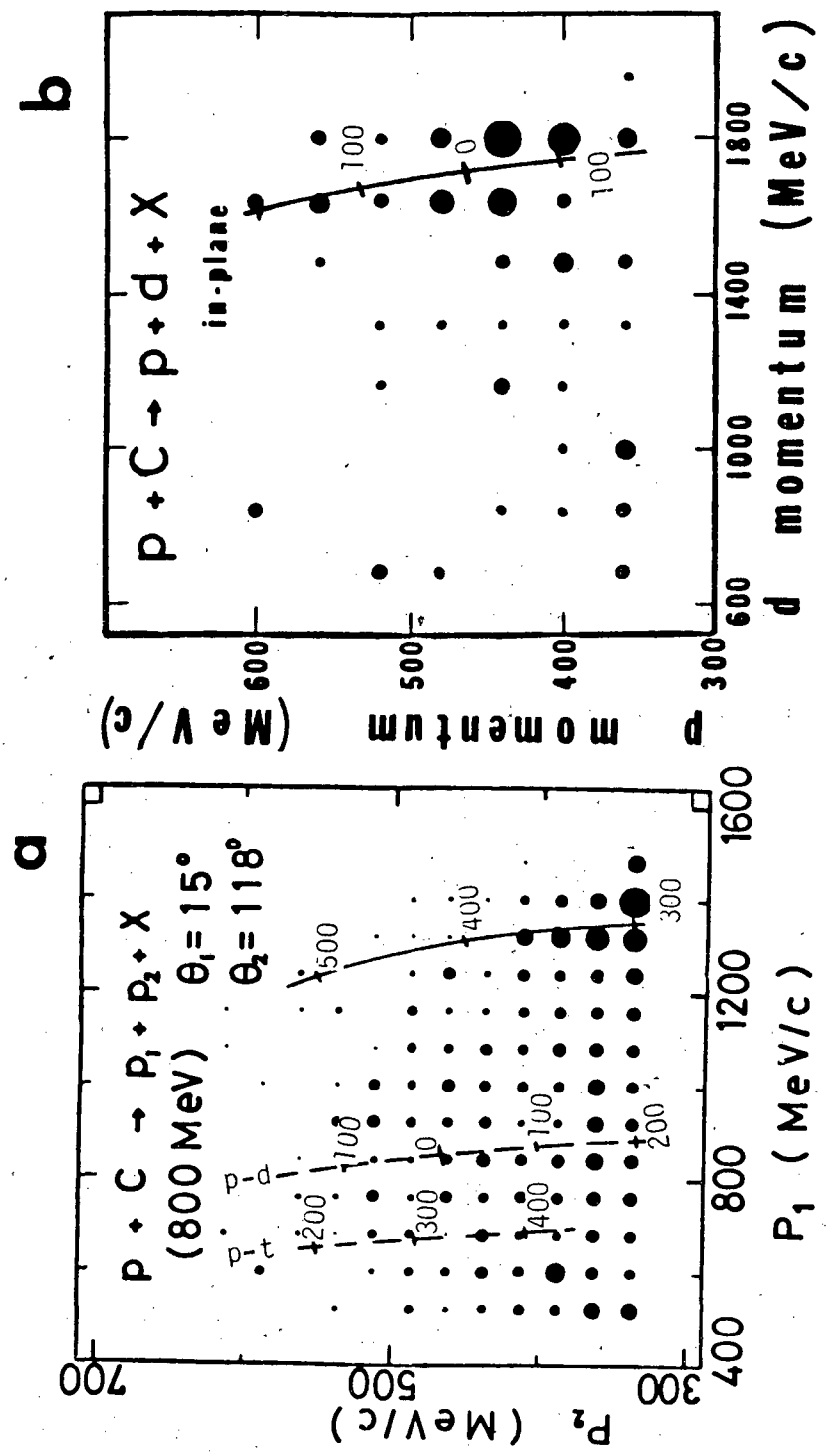

XBL 817-10845

Fig. 21

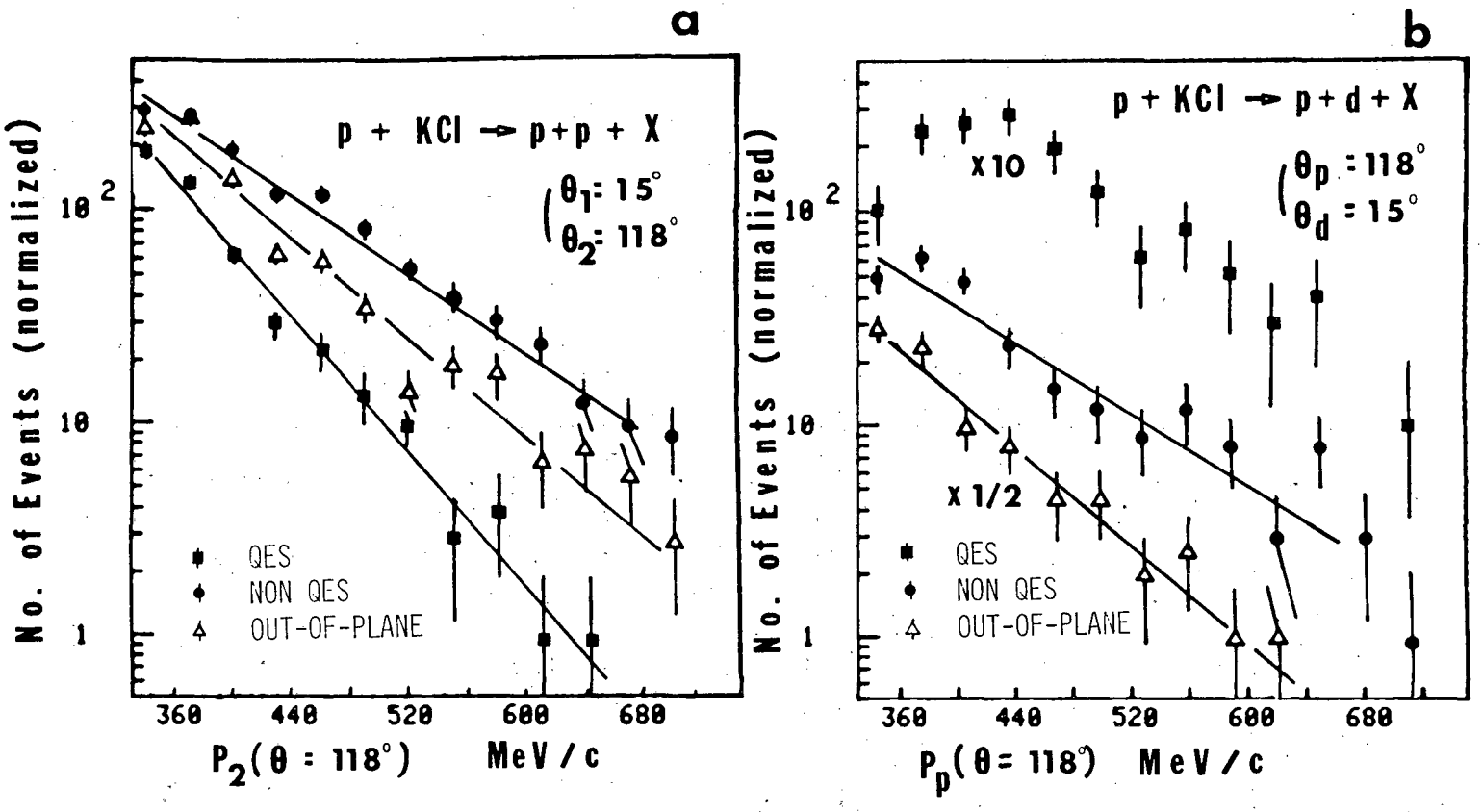

XBL 817-10846

Fig. 22

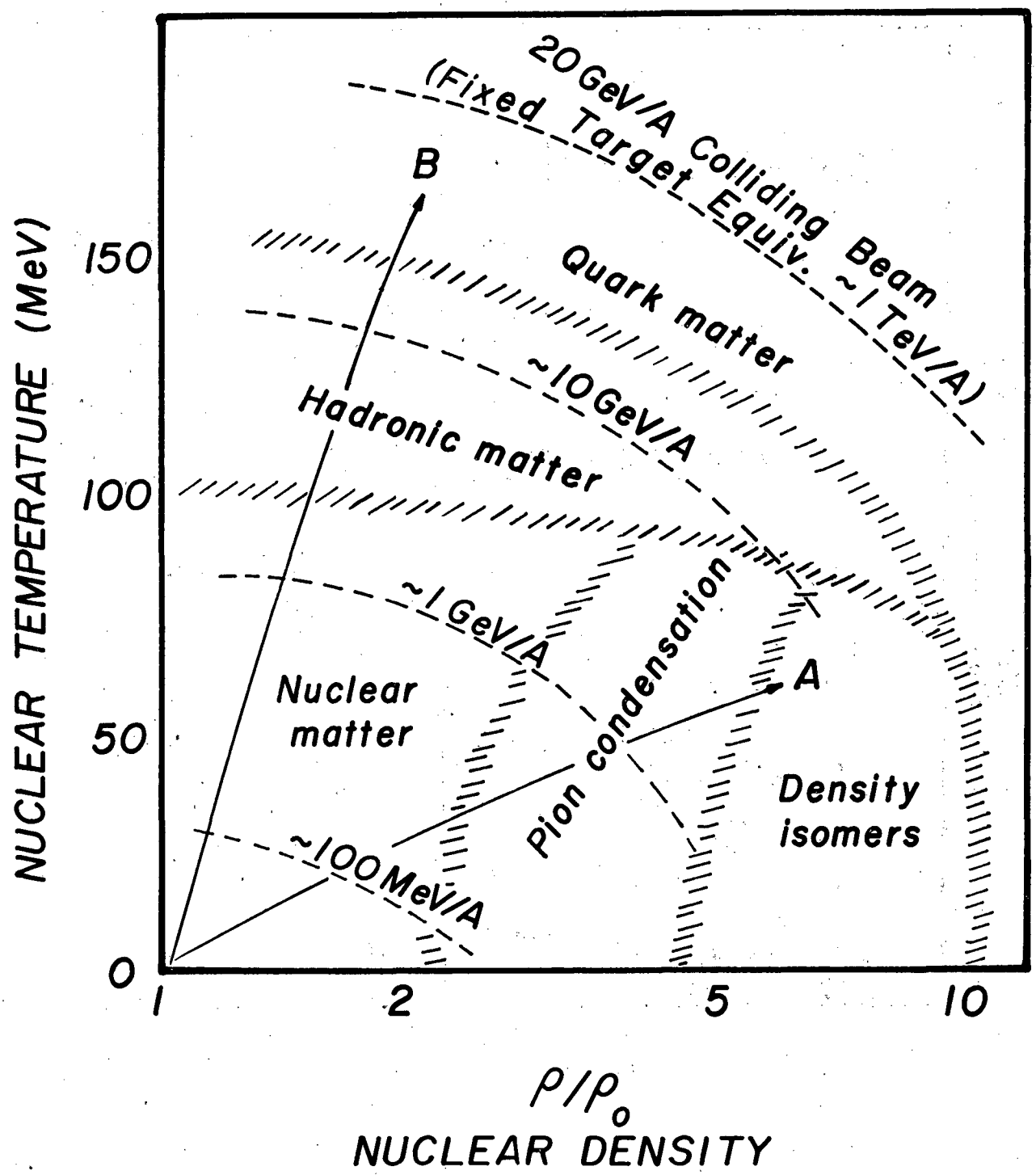

XBL 7910-12108

Fig. 23

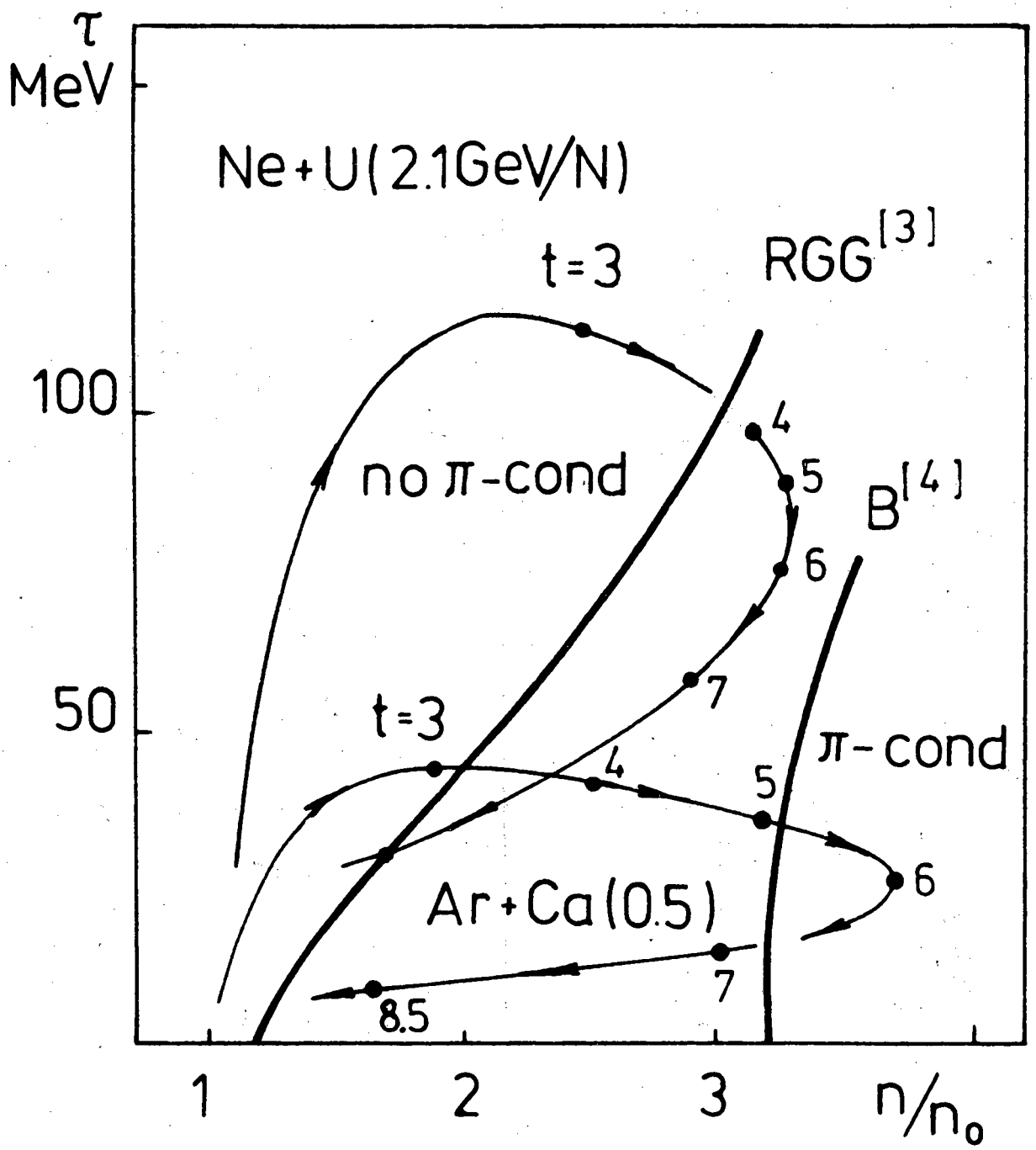

XBL 805-9542

Fig. 24

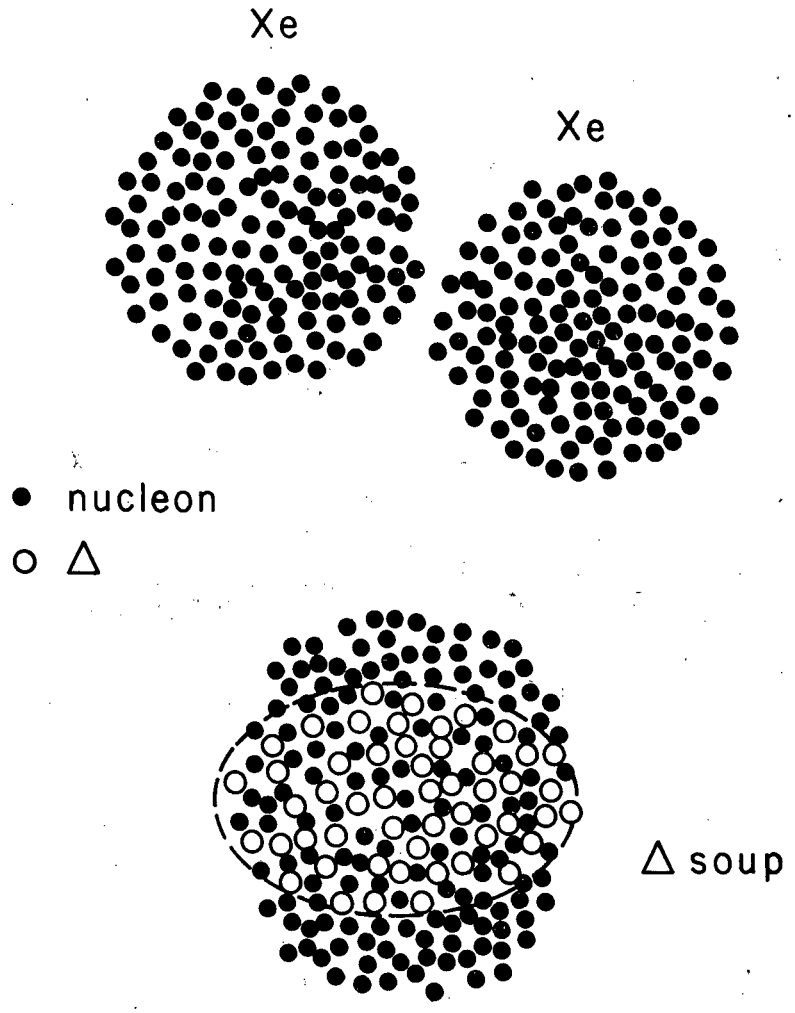

XBL 821-74

Fig. 25

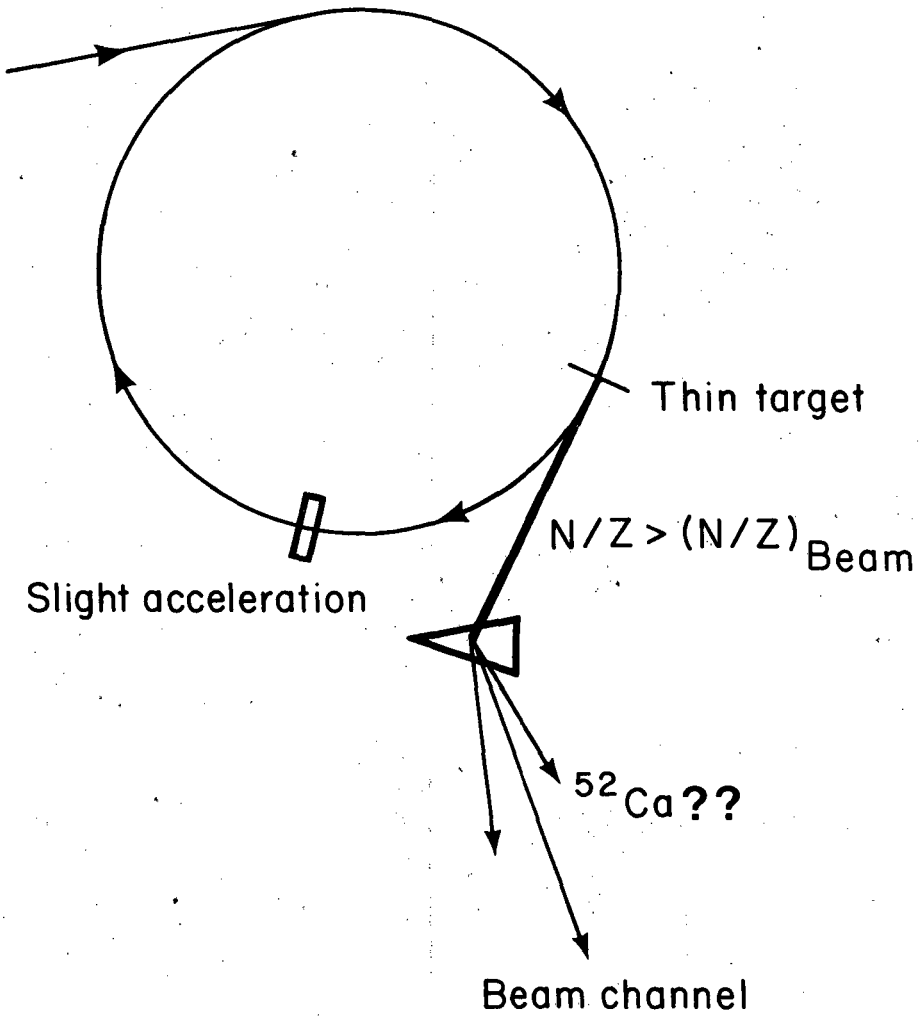

XBL 821-80

Fig. 26

TECHNICAL INFORMATION DEPARTMENT
LAWRENCE BERKELEY LABORATORY
UNIVERSITY OF CALIFORNIA
BERKELEY, CALIFORNIA 94720